DISORDERING KINETICS IN ORTHOPYROXENES

by

James R. Besancon

B. S., Yale University (1969)

Submitted in partial fulfillment

of the requirements for the

Degree of Doctor of

Philosophy

at the

Massachusetts Institute of Technology

May 12, 1975

Signature of Author.....
Dept. of Earth and Planetary Sciences

Certified by.....
Thesis Supervisor

Accepted by.....

WITHDRAWN FROM MIT LIBRARIES
SEP 24 1975
LIBRARIES

by

James Robert Besancon

Submitted to the Department of Earth and Planetary Sciences in May 1975, in partial fulfillment of the requirements for the degree of Doctor of Philosophy

ABSTRACT

Isothermal heating of a quasibinary orthopyroxene, $Mg_{1.70}Fe_{.26}Ca_{.02}Al_{.04}Si_{1.96}O_6$ resulted in increasing Fe^{2+} - Mg^{2+} disorder, which was measured by Mossbauer spectroscopy. Several pieces of equipment were designed for this study, including a multiple-sample, independent quenching, electric furnace, with oxygen fugacity controlled by gaseous buffering mixtures, and a vibration-damping table for the Mossbauer spectrometer.

Minimum values of equilibrium disorder are higher than predicted by ideal solution models. The Saxena-Ghose (1971) model is applied to existing disorder data at 700°C and 800°C, and activity coefficients calculated by least squares fitting. Energy parameters for the model are found to be W_{M1} = 2.3 kcal, and W_{M2} = 2.0 kcal. At 800°C, ln K = -.98 and at 700°C, ln K = -1.24. Because the energy parameters are almost independent of temperature, the excess entropy of mixing is small.

The progress of disordering with time did not follow traditional rate equations, or any two-step models; the rate fell more quickly. A modification is proposed to Mueller's (1969) model, incorporating activity coefficients, showing explicitly the dependence of rate on difference in chemical potential. At 750°C and 800°C, disordering passed through a maximum and decreased slowly, suggesting a competing process. A hypothesis is advanced that dissolution of shear-induced lamellae of clinopyroxene may be the cause of the maximum, and possibly of the

declining rate at 700°C.

A comprehensive defect model for orthopyroxene is proposed, which may be used as a framework to understand transport processes and other phenomena. The dependence of defect concentration on oxygen fugacity is shown. Increase in oxygen fugacity results in an increase in rate of disordering, pointing to cation vacancies as the important species involved.

Application may be made to rapid natural processes, such as cooling rates of volcanic rocks and emplacement of kimberlites. Preliminary data suggest that kimberlite was very rapidly quenched from high temperatures.

An appendix discusses factors affecting the intensity of Mossbauer peaks.

Thesis Supervisor

Roger G. Burns

Professor of Geology and Geophysics

TABLE OF CONTENTS

Chapter 1 - Introduction	p.9
Chapter 2 - Experimental Design	p.14
Chapter 3 - Mossbauer Spectrum Methodology	p.46
Chapter 4 - Disordering Data	p.58
Chapter 5 - Discussion of Equilibrium Distributions	p.68
Chapter 6 - Defect Equilibrium and Disordering	p.73
Chapter 7 - Isothermal Disordering with Time	p.90
Chapter 8 - Applications of Order-Disorder in Orthopyroxenes to Natural Processes	p.106
Appendix A	p.111
Appendix B	p.113
Bibliography	p.124

TABLES

1 p. 16 Microprobe analyses of pyroxene and chromite inclusion.

2 p. 28 Typical flow rate data for capillaries.

3 p. 54-55 Disordering data

4 p. 71 Parameters from least squares fit of distribution data to Saxena-Ghose model.

5 p. 83-84 Variation of native imperfections under varying neutrality and anion partial pressure conditions.

FIGURES

1 p. 23 Gas mixing apparatus

2 p. 29 Bunsen bubble tower for gas flow measurements

3 p. 32 Quenching furnace, schematic

4 p. 33 Gas inlet system for furnace

5 p. 38 Samples attached to furnace head

6 p. 40 Furnace head joint

7 p. 49 Mossbauer spectrometer support table

8 p. 57 Representative Mossbauer spectra

9 p. 59 Disorder vs. time, 700°C

10 p. 60 Disorder vs. time, 750°C

11 p. 61 Disorder vs. time, 800°C

12 p. 62 Disorder vs. time, 700°C, semilogarithmic plot

13 p. 87 Variation of native imperfections with R.

14 p. 97 Model calculation of disorder vs. time, 700°C

15 p. 98 Model calculation of disorder vs. time, 800°C

16 p.101 Sketch of pyroxene octahedral chain

17 p.115 Quadrupole moment diagram

The heavens themselves, the planets, and this centre
Observe degree, priority, and place,
Insistiture, course, proportion, season, form,
Office, and custom, in all line of order.

W. Shakespeare, Troilus and Cressida
I. iii.

I know a planet where there is a certain red-faced gentleman. He has never looked at a star. He has never loved any one. He has never done anything in his life but add up figures. And all day he says over and over, just like you: 'I am busy with matters of consequence!' And that makes him swell up with pride. But he is not a man - he is a mushroom!

Antoine de Saint Exupery, The Little Prince

ACKNOWLEDGEMENTS

Financial support for this thesis came from the Department of Earth and Planetary Sciences, which funded much of the equipment expenditures. Professor R. G. Burns also provided significant material aid.

Personal support came from teaching and research assistantships at MIT, from a Sloan fellowship, from New England Nuclear Corp., and from the University of Rhode Island.

Technical help and discussions with the following people were an invaluable aid in the completion of this thesis:

Dr. A. Duba, Dr. E. Whipple, Prof. N. Gray, Prof. S. Hafner, Dr. F. Huggins, Dr. R. Abu-Eid, Mr. K. Goettel, Mr. D. Skibo, Dr. J. Chernosky, Dr. D. Wones, Prof. C. Goetze, Dr. T. McGetchin, Prof. P. Hurley, Dr. D. Kohlstedt, Prof. W. Pinson, Prof. H. Fairbairn, Prof. F. Frey, Prof. J. Dickey, Prof. D. Vaughan, Prof. J. Tossell, Mr. W. Menke, Mr. C. Sung, and Mrs. V. Burns.

My wife has been an inspiration and help in many ways, too numerous to mention.

Chapter 1 INTRODUCTION

As a result of the solution of the crystal structure of enstatite (Warren and Modell, 1930), it is now known that there are two crystallographic sites in orthopyroxene, of different symmetry, which can accept either magnesium or iron. Ghose (1965) confirmed, by x-ray crystal structure refinement, his earlier predictions (Ghose, 1962) that ferrous iron is enriched in the more distorted of the two octahedral sites in hypersthene, the site designated M2. This discovery provoked a spate of interest in cation distribution studies as a possible geothermometer, and as a modifier of intercrystalline equilibria involving iron and magnesium exchange with coexisting olivine.

Interest in site occupancies led to attempts to find better ways of measuring the site populations of orthopyroxenes, the x-ray diffraction method being costly and time consuming. The method showing the most promise was the Mossbauer effect, the resonant absorption of nuclear gamma rays emitted by an excited state of iron-57 and absorbed by naturally occurring iron-57 in the pyroxene (Bancroft et al., 1967; Marzolf et al., 1967; Evans et al., 1967; Ghose and Hafner, 1967). Iron in the two different sites showed different Mossbauer parameters so that separate doublet absorption peaks arose from each site. The relative areas of the respective doublets were assumed to be an accurate measure of the proportion of ferrous iron in the two sites, an assumption which was borne out by later studies (Virgo and Hafner, 1970; Burnham et al., 1971).

In addition, the amount of ordering of iron was shown to be temperature dependent (Evans et al., 1967; Ghose et al., 1967).

As a result of these preliminary measurements, a series of experiments was undertaken by Virgo and Hafner to determine the temperature dependence of the ordering and disordering reactions, and any effect the rate of exchange might have. In a classic paper, Virgo and Hafner, (1969) obtained data and developed a theory of ordering in a number of heated orthopyroxenes which provided a consistent and useful picture of the nature of the ordering reaction and disordering reaction. They also described some preliminary data on the rates of those reactions. A consistent thermodynamic theory, based on work by Mueller (1962, 1967), Matsui and Banno (1965), and Grover and Orville (1969), was presented that showed an approximately constant energy of exchange between the two sites in the temperature and composition range examined.

Virgo and Hafner (1969) had obtained the rate data on two orthopyroxenes, of composition fs .57 and fs .3209, in a series of disordering experiments. The activation energy of the reaction was estimated to be about 20 kcal per gram formula weight, using the kinetic model of Mueller (1967, 1969). The rate constants determined at 500°C were about the same for both ordering and disordering, leading to a suspicion on their part that the model was inadequate, but further data were needed to analyze the problem.

Virgo and Hafner (1970) further delineated the cation distributions in naturally occurring orthopyroxenes, and showed that the degree of

ordering corresponded to temperatures that were often lower than would be predicted by independent means such as petrogenesis. Additional studies by Dundon and Hafner (1971) showed that shock treatment of pyroxenes increased the observed disorder. Burnham et al. (1971) investigated the correlation between site population estimates obtained from x-ray crystal structure refinements and Mossbauer spectroscopy, and found quite good agreement between the two methods. They also investigated the thermal vibrations in the pyroxenes examined.

Saxena and Ghose (1971) repeated some of the experiments of Virgo and Hafner, and presented a thermodynamic model based on the work of Guggenheim on regular solutions. Their results were in general agreement with those of Virgo and Hafner, but their model took into account the nonideality of the solution. This work was elaborated on by Saxena (1973), who reviewed the relevant aspects of Guggenheim's theory.

A somewhat different approach was taken by Navrotsky (1971), who calculated the configurational entropy using methods of statistical mechanics. She showed that the solution, at least so far as the data of Virgo and Hafner, could be understood in terms of simple ideal solution, the negative enthalpy of mixing being offset by a negative entropy of mixing. The calculation of the configurational entropy is similar to that of Brown (1971), who derived the general equation for entropy in ordered plagioclase , but not pyroxene.

Much work on the kinetics of the ordering and disordering processes in minerals is contained in the papers of Mueller (1967, 1969, 1970),

who modified the theory of Dienes (1955). The assumption made is that the ordering rate follows Fick's laws of diffusion, the rate being dependent on the degree of order (or disorder) already achieved by the system. A theory developed by Vineyard (1956) used a set of distribution functions to describe the array of atoms in various configurations, and was able to show the time dependence of long range order in nonequilibrium situations. This theory converges to the results of Bragg and Williams (1934) and Dienes (1955) at equilibruim. Another virtue of the Vineyard theory is that it is able to discuss diffusion by either direct interchange mechanisms (physically unlikely) and vacancy mechanisms (a possible mechanism in pyroxenes). The major problem of the Vineyard theory is that it is difficult to apply to complex crystal structures, and differential equations arising from it are difficult to solve. As discussed by Mueller for the case of Dienes' model, the usual metallurgical assumption that the energy term in ordering depends on the degree of ordering is probably invalid for the case of oryhopyroxenes, because the silicate framework (and therefore the anions) remains essentially fixed no matter what the degree of ordering. The energy per interchange of Mg and Fe between M1 and M2 sites is probably fixed by the geometry of the sites, and is little affected by the nearest cations which are really second nearest neighbor atoms. This assumption can simplify significantly the Vineyard theory.

The most recent useful work on ordering and disordering rates in orthopyroxenes is the work of Gray (1974), who used a geometric model

based on the work of Vineyard. His theory is able to predict the direction of variation of rates from the equilibrium, Dienes - Mueller type, models. Unfortunately, it can not be applied quantitatively to experimental results because the parameter used in the calculation is based on physical and geometrical theory and can not be measured directly by either x-ray diffraction or Mossbauer techniques. It is related to non-equilibrium distributions on a microscopic scale.

Further work of some relevance to ordering rates in pyroxenes was done by a number of workers on feldspar ordering, which shows some qualitative similarities to the orthopyroxene case. The ordering examined here is Si - Al ordering in tetrahedral sites. Holm and Kleppa (1968) showed that the rate can be described as a two-step process in albite, with final equilibrium taking much longer (40+ days at 1000°C) than the faster initial equilibrium. An important paper applicable to the present thesis is that of Smith and Ribbe (1969), who discussed ordering in plagioclase feldspars, an ordering process that is strongly affected by the presence of domain structure and structural changes across the compositional range of the feldspars.

The present study was initiated in order to investigate in more detail the kinetics of disordering reactions in orthopyroxenes. Evaluation of rate controlling factors was the major goal.

Chapter 2 EXPERIMENTAL DESIGN

Because ordering reactions in general seem to be controlled by diffusion rates of the relevant atomic species between crystal sites, the normal factors controlling diffusion were considered. They are temperature, pressure, major element composition, trace element content, structure, surface area, and partial pressure of both the major elements and possible catalysts like hydrogen. As all of these factors could not be fully investigated in one thesis, the ones thought to be most important have been examined: temperature, and partial pressures of major and possibly catalytic atoms.

The major element composition factor is examined only indirectly, by comparing with the results of Virgo and Hafner, (1969), and Khristoforov et al., (1974). The effect of pressure, while relevant, was experimentally intractable if oxygen fugacity was also to be controlled. Trace element content was entirely too complex for kinetic analysis, even in supposedly "pure" synthetic pyroxenes and usually does not alter the basic mechanisms of diffusion of major ions.

For imperfections in the lattice caused by "foreign" ions, the number of impurity atoms is larger than the number of solvent atoms disturbed by the surfaces present (in macroscopic crystals) until the impurity level reaches one part in 10^8 or less (Flynn, 1972). Thus surface effects (surfaces are usually high diffusion rate paths) are much more important than impurities for most processes that occur in even the

purest synthetic minerals. Sample preparation minimized surface area produced by crushing and grinding, and the sample was homogeneous in size distribution, but surface area was not measured as an independent variable.

The experimental design was chosen with these factors in mind. In order to make the system as simple as possible, the first major decision involved choice of sample. Ideally, it should lie in the binary system $MgSiO_3$-$FeSiO_3$, with little substitution of calcium, manganese, titanium, or aluminum. In order to keep the compositional factors as constant as possible, enough sample was required to perform all the heating experiments on homogeneous, sized splits from one original sample. In addition, it was desired that the composition lie in the bronzite range, making it similar to some pyroxenes obtained from kimberlite xenoliths. In this way, the data could perhaps be applied to models of kimberlite emplacement (McGetchin and Ullrich, *1973*), which call for rapid cooling by adiabatic expansion.

Such a sample was located in the M.I.T. collection after a screening by optical and atomic absorption analysis of several samples. The orthopyroxene is an almost completely monomineralic specimen from Harford County, Maryland, hereafter designated HCo. Electron microprobe analysis (Table 1) verified the quasibinary nature of the sample, the absence of zoning, and almost complete absence of macroscopic clinopyroxene exsolution lamellae. Optically, the sample is homogeneous except for a very few exsolution lamellae, very tiny blebs of chromium iron spinel (analysis,

Table 1
Microprobe Analyses

Sample HCo:

Oxide	Wt.Percent	Cation (basis 6 oxygens)
CaO	0.59	0.021
TiO_2	0.11	0.002
Na_2O	0.02	0.001
MgO	32.42	1.702
Al_2O_3	1.07	0.043
SiO_2	55.65	1.960
Cr_2O_3	0.41	0.011
MnO	0.22	0.006
FeO	8.74	0.257
	99.22	4.004

Opaque inclusion in HCo (Chromite)

Oxide	Wt.Percent	Cation (basis 4 oxygens)
CaO	0.00	0.000
TiO_2	1.16	0.039
Na_2O	0.00	0.000
MgO	1.43	0.096
Al_2O_3	0.94	0.049
SiO_2	0.40	0.017
Cr_2O_3	23.76	0.852
MnO	0.47	0.017
FeO	63.54	2.412
	91.70	3.481

(Above analysis then recalculated, proportioning iron between ferric and ferrous components:

$$(Fe^{2+}_{1.91}Mg_{.09})(Fe^{3+}_{1.21}Cr^{3+}_{.75}Al_{.04})O_4 \quad)$$

Table 1), and a number of shear planes. The calcium content of the sample as measured by atomic absorption agreed quite closely with the value obtained by electron microprobe, suggesting that the sample contains most of the calcium within the orthopyroxene phase rather than in the very minor exsolved clinopyroxene.

Examination of sample HCo by transmission electron microscopy showed many planar features superimposed on the regular 14Å spacing of the (100) planes. These are interpreted as shear features resulting from solid state deformation of the pyroxene. The exact nature of structures such as these has been debated in the literature; they have been interpreted both as stacking faults and as small included areas of clinopyroxene. Buseck and Iijima (1974) have fairly strong evidence that the latter is sometimes true. They interpret the planar features observed in the Norton County enstatite as clinopyroxene induced by the shock that produced the observed brecciation. This agrees with the findings of Turner, Heard and Griggs (1960), who reported the stress induced transition from orthoenstatite to clinoenstatite. No quantitative measure of the abundance of these shear features was made, but their volumetric significance is relatively low. During experimentation, temperatures were kept low enough that protoenstatite should not have appeared, because on quenching it would have produced significant quantities of clinoenstatite. However, the temperatures used should have annealed much of the clinoenstatite and converted it to orthoenstatite, which is the thermodynamically stable phase in this temperature range. This annealing has been

observed by Boland et al. (1974), during experimentation on the electrical conductivity of orthopyroxene, and will be discussed with the results of the present thesis.

The symmetry of the sample obtained was assumed to be orthorhombic, but no crystal structure analysis was attempted. In order that the field of stability of orthopyroxene not be exceeded, the temperature of all experiments was kept below 1000°C, as the effect of a gross structural rearrangement would almost certainly alter the disordering process. The stability field of orthopyroxenes in that region has been investigated by Smyth (1971). Other information of the structure and stability of orthopyroxenes can be found in Smith (1969), Smyth (1969), Smyth (1970), Smyth and Burnham (1972), Smyth (1973), and Nitsan (1974).

A natural mineral was chosen for the experiments rather than a synthetic one because of the ready availability of large quantities of homogeneous material produced under essentially identical conditions, particularly an identical temperature history. The presence of small amounts of elements not present in the pure binary system was of somewhat less importance than other factors. A further advantage in using a natural mineral derived from a metamorphic environment is that extensive ordering over a long time period had taken place, a situation not easily achievable in the laboratory for a synthetic sample of relatively large size. The highly ordered natural sample made the changes in degree or ordering on heating larger than would be possible for a more disordered, laboratory produced sample. This ensured that the high-

est possible precision in measurement would be achieved.

The control of the partial pressure of major ions and catalytic ions is a major advance in the study of ordering kinetics of orthopyroxenes. As mentioned above, it is thought that possible mechanisms responsible for diffusion (and rearrangements like ordering) are the movement of vacancies or of interstitial atoms through the structure. It should be possible to verify the machanism as resulting either from vacancy diffusion or by interstitial movement, by measuring the effect of increasing or decreasing the number of vacancies present. As will be discussed in a later section, this number of vacancies can be controlled by the activity of either the cation or anion in the environment around the crystals.

The factors described in chapter 1 necessitated the design of apparatus for heating samples to the required temperatures. Other requirements included long term temperature stability, maximum precision in sample treatment, rapid quenching, and long term oxygen fugacity control. Economy of construction was also a major factor in design, as the budget for equipment was quite low.

At first, solid phase oxygen buffers were considered, which consisted of mixtures of metal and metal oxides that control the fugacity to a calculable value at a given temperature. Because of the limited variability of the system, and the added complication of using a double capsule, this was finally rejected. Another factor legislating against this type of system is that reliance must be made on hydrothermal appar-

atus instead of a simpler furnace arrangement. The optimum arrangement then seemed to be buffering using gas mixing, with systems such as CO - CO_2 or H2 - CO_2.

The basic idea of using gas mixtures like these is that high temperature dissociation of the gases (or their reaction products like H_2O) releases a very small amount of oxygen, which is available to react with solids present. Assuming that equilibrium with the solid is achieved, partial pressure of oxygen in the solid is controlled. In the present case, the CO_2 - H_2 mix was used as the basic mix because of the low cost of these gases relative to CO (about $50 for a cylinder containing 200 cubic feet). The equations necessary for calculating the equilibrium in this system are found in Muan and Osborn (1965) and in Nafziger et al., (1971), and will only be outlined here.

The method consists of using tabulated thermodynamic data for the free energy of formation of the gases involved, and calculating the equilibrium constants for the possible reactions between them. These equilibrium constants can then be related by the stoichiometry of the reactions to the partial pressure of oxygen. The important equations for the H_2 - CO_2 system are:

(1) $CO_2 = CO + \frac{1}{2} O_2$

and

(2) $H_2O = H_2 + \frac{1}{2}O_2$.

The equilibrium constants for these equations are, respectively,

(3) $K_1 = \dfrac{f_{CO} f_{O_2}}{f_{CO_2}}$ and

$$(4)\quad K_2 = \frac{f_{H_2}\, f_{O_2}^{\frac{1}{2}}}{f_{H_2O}}$$

Assuming the fugacity is equivalent to the partial pressure of these gases in a mixture at one atmosphere, and that the sum of the partial pressures of the gases CO, H_2O, CO_2, and H_2 is unity at one atmosphere (ignoring other possible species like CH_4, French (1966)), one can write the equation:

$$(5)\quad \frac{pCO_{2(i)}}{pH_{2(i)}} = \frac{1 + \frac{pCO_2}{pCO}}{1 + \frac{pH_2}{pH_2O}}$$

where $\underline{i}$ denotes the initial quantities of each gas. This can then be recast as:

$$(6)\quad \frac{f_{CO_{2(i)}}}{f_{H_{2(i)}}} = \frac{1 + \frac{f_{O_2}^{\frac{1}{2}}}{K_1}}{1 + \frac{K_2}{f_{O_2}^{\frac{1}{2}}}}$$

A simple Fortran IV program was written to provide tabulated values of the volume percent CO_2 in a mixture of H_2 and CO_2 that would produce a given oxygen fugacity at a given temperature. The program (Appendix A) uses equation 6, assuming that the values of free energy of formation of the gases involved can be linearly extrapolated for temperatures between the 100°K values given in most compilations, an approximation that is overshadowed by other errors in the experimental setup. Any

consistent set of free energies can be plugged into the data section of the program, such as that of Coughlin (1954) or Elliott and Gleiser (1960). However, the set used (differing very little from the above two) is taken from Robie and Waldbaum (1968). Equilibrium constants follow from $\Delta G=-RT\ln K$, where ΔG is the difference in free energies, and K the equilibrium constant. A better set of tables for both H_2 - CO_2 and CO - CO_2 has recently become available (Deines et al., 1974), and these are used in this thesis.

The next concern in experimental design was to achieve accurate delivery of a stream of gases mixed in precisely the ratio desired with reasonable long term stability and reproducibility. The design chosen for a gas mixer is based on that of Darken and Gurry (1945), as modified and described by Nafziger et al.(1971). The important feature is that the gases are applied at a constant pressure against one end of a capillary, and the resulting flow rate through the capillary is proportional to the applied pressure, and is <u>linearly</u> proportional within some experimentally useful range. By setting the pressure drop across a capillary to some predetermined value and allowing any excess gas to bleed off, a constant and continuously adjustable flow can be achieved through the capillary. By setting up a separate capillary for each gas, the ratio of the two can be varied within the limits set by the linear flow regime of the capillaries.

A schematic diagram of the gas mixer is illustrated in Figure 1. The pressure drop across the capillaries is monitored by U-tube mano-

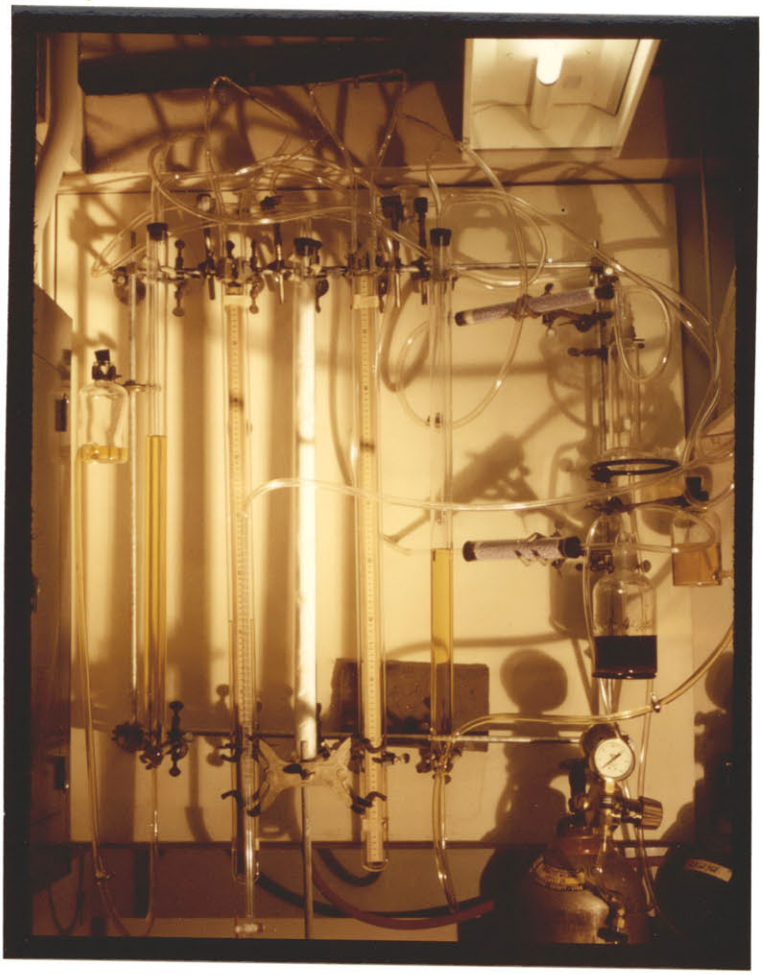


Figure 1 Gas mixing apparatus. System is symmetrical, with light colored central tube being the mixing tube, then the manometers, then the overflow bubble tubes.

meters, which are calibrated against flow rate, as described below. An inexpensive and convenient fluid for indicator liquid is high grade vacuum pump oil, which has an extremely low partial pressure, is chemically stable, and has a low density which makes possible use of relatively larger and stronger capillaries because the required pressures are low. If mercury were used as manometer liquid, extremely fine capillaries would be needed to provide the relatively low flow rates used in the experiment.

The gases are combined in a one inch tube packed with glass wool for thorough mixing. The resultant mixture is led out through high vacuum rubber tubing to minimize differential diffusion, which might alter the mixing ratio of the two gases.

Excess pressure of each gas is applied to the system, but this is reduced by the needle valve on the gas cylinders and by a bubbler. This consists of two concentric glass tubes, with the outer tube filled to an adjustable level (set be raising or lowering an external reservoir) with pump oil. Gas flowing into the inner tube forces the oil out until gas is bubbling up through the oil in the outer one. At this point, the pressure of gas in the inner tube is relatively insensitive to fluctuations in the applied pressure, as any excess gas simply results in an increase in bubbling rate, and a paucity of gas results only in a decrease in bubbling. This then is the constant pressure which is applied to the capillary.

The apparatus is made primarily of glass. Great economies of con-

struction can be made by simply interconnecting standard glass parts with small sections of Tygon tubing. Some care must be exercised in use of Tygon, as CO_2 diffuses through it even though it is impervious to hydrogen, the rate being dependent on wall thickness and length of tubing (Nafziger et al., 1971). If the amount of tubing is kept to a minimum and is in place during calibration of the apparatus, there should be no real problem.

Capillaries are usually custom constructed for use in the apparatus by drawing out commercial heavy walled capillary tubing to smaller diameters. If the constriction of the tube is carefully done, the resultant flow rate - pressure relationship is linear over a larger range of pressures, and the capillary is correspondingly more useful. Constrictions of about $\frac{1}{4}$ millimeter proved to be the correct range, but trial and error is the only way for deciding on the utility of any individual capillary made. Fancier constructions, which allow easier interchange of capillaries than simple Tygon connections, can be made if a glassblower is available. Designs for some of these capillary systems are shown in Nafziger et al. (1971).

Stopcocks or screw clamps can be added in several places to facilitate the setup of a given flow rate. These include one between each reservoir for the bubbler fluid and the bubbler itself to keep the fluid level constant, and two more which isolate the two sides of the mixer from each other to aid in calibration.

In practice, the gas flowing into the mixer is adjusted until the

bubbling rate is slow and steady, and the pressure is read off a scale set by the manometer. To increase the flow rate, the bubbler reservoir is raised and the level of fluid in the bubbler is increased, creating a higher head pressure. The flow into the system is then increased until the slow bubbling rate is again achieved. By manipulation of the reservoir fluid, the pressure can thus be set to any value of the manometer.

With capillaries in the $\frac{1}{4}$ millimeter range, the requisite flow rate of 0 to 4 cm^3/sec was easily achieved with bubbler tubes about one meter long, and resulting differential pressures on the manometer of about 50 cm of pump oil.

The entire mixer was mounted on a board which was firmly attached to a wall. The glass was attached by standard laboratory clamps (kindly provided by Prof. P.M. Hurley) to metal rod frames which were set about four inches from the board. Some way must be provided to get access to the capillaries at the top of the system so that they may be changed. Care must be taken when changing capillaries not to restrict significantly the Tygon tubing, otherwise the flow regime may either lose calibration or simply always be nonlinear.

Calibration is accomplished with a Bunsen bubble tower. This consists of a broken burette, the fine tip being completely removed. Gas is led into one arm of a Y shaped tube at the bottom, and allowed to pass through the other arm of the tube and then up the burette. Soap bubble solution (several preparations were tried but commercial children's

bubble solutions proved to be the best) is introduced through the base of the Y. The level of solution is raised until one or several bubbles are produced and begin to rise through the burette. The time required for a given volume of gas (typically about 50cm3) to rise was measured with a stopwatch. Ten duplicate runs (or five in the case of unusually low flow rates) were made at each calibration flow rate for each gas and each capillary used. Some capillaries proved to have nonlinear flow rate - pressure relationships and were not used; others proved to be quite suitable. Flow rate data points for about five or more pressures were measured on each capillary that was finally used, and fitted by a least squares fitting routine to a straight line function, which was then used during setup to find the pressure required for a specified flow rate. Deviations from linearity were checked by graphical analysis of the data, which showed the linear portions of the flow regime. The flow rate data for the capillaries used are summarized in Table 2. Figure 2 is a schematic diagram of the bubble tower.

The optimum flow rate for gas mixing furnaces which minimized thermal diffusion (causing unmixing of the gases) and temperature uncertainties was obtained from Darken and Gurry (1945). For a one inch furnace tube (such as that used in this study) and a twelve inch long heated zone, the optimum flow rate is 0.9 cm/sec through the tube, or a total flow of 4 cm^3/sec. This total flow rate was used in all experiments, proportioned between the two gases.

Gases need to be purified and dried before they are introduced

Table 2
Typical flow rate data for capillaries

CO_2, Capillary A1, left side of mixer.

Manometer Pressure (cm oil)	Flow rate (cm^3/sec)
36.35	1.525
31.85	1.333
48.15	1.973
23.95	0.978
19.10	0.781
15.00	0.637
32.75	1.312
44.15	1.768

H_2, Capillary A2, right side of mixer.

Manometer pressure (cm oil)	Flow rate (cm^3/sec)
14.45	1.020
20.60	1.459
31.00	2.222
41.90	3.014
19.00	1.359
13.50	0.942
8.90	0.621
3.75	0.249
1.65	0.101

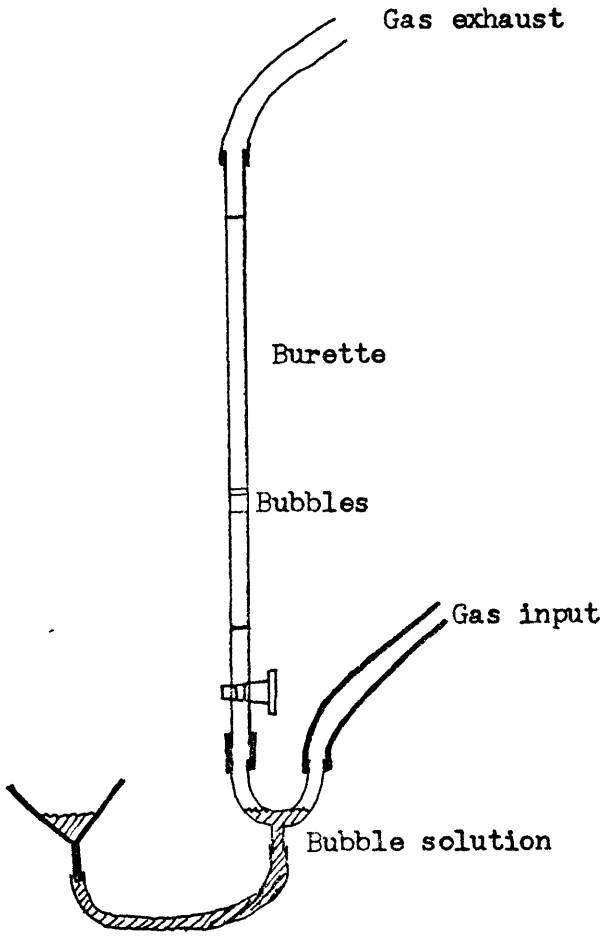


Figure 2 Bunsen bubble tower for gas flow measurements

into the mixer. Hydrogen is normally just dried by passing through a tube packed with Drierite ($CaSO_4$ to which an indicator is added that shows when the drying capacity is expended). CO_2 is oxidized to eliminate any hydrocarbons or carbon monoxide. Previous investigators have used heated copper gauze and activated Al_2O_3 with Drierite to remove water. At the suggestion of Earle Whipple, this system was replaced by one in which CO_2 was bubbled through a chromic acid cleaning solution (made by adding potassium dichromate crystals to concentrated sulfuric acid) which very effectively both oxidizes and dries the gas. As a precaution to remove the cleaning solution, the gas was then passed through a Drierite tube. This system was shown by Whipple to result in improved chemical purity for the CO_2, as demonstrated by lessened reducing power when used as covering gas during ferrous iron determinations (Whipple, 1973). Carbon monoxide was cleaned with sodium hydroxide pellets, which both dry the CO and remove CO_2.

From the gas mixer, the gases are led into the furnace system. This was designed with economy in mind, as well as maximum utility and reproducibility of results. The most important features of the furnace design were: the ability to run seven samples at a time, with temperature measured at all times in a symmetrically equivalent site in the furnace; complete sealing against contamination of air; cooling of exit gases to allow venting into a hood duct; and independent rapid quenching of each sample. The advantages of running multiple samples are great: all samples in the run experience the same conditions of temperature

and oxygen fugacity; as well as the same temperature history during initiation of a run; and great economy is achieved in equipment usage and time.

An electrically heated furnace mounted in a vertical position was used. It was cylindrical, wound with Kanthal wire, and had an 18 inch heated zone. The length of the heated zone was probably a positive factor in promoting equilibration of the gases in the mix before they reached the sample area. The opening in the ceramically lined tube was about $1\frac{1}{2}$ inches in diameter. Inside this, a tube of fused silica was placed, which was the actual furnace tube. The 1" diameter silica tube projected about one foot from each end of the furnace, and allowed the connections of gas and sample support to be somewhat insulated from the furnace area and maintained at a reasonable low temperature (Figure 3). Silica was chosen because of its good radiative thermal conductivity and becauses it contributes negligible contamination to the sample. A ceramic tube could easily be used instead. The vertical configuration was best because it allowed the simplest quenching of samples.

The gas inlet system (Figure 4) was designed as a two gate valve airlock, so that samples could be removed from the furnace without allowing contamination of the gas stream by air, which would not only upset the gas buffering but might be dangerous in the presence of hydrogen. The original plan was to use liquid nitrogen as a quenching fluid, because it would be essentially inert in the system and would not have the toxicity problems associated with mercury, the traditional quenching

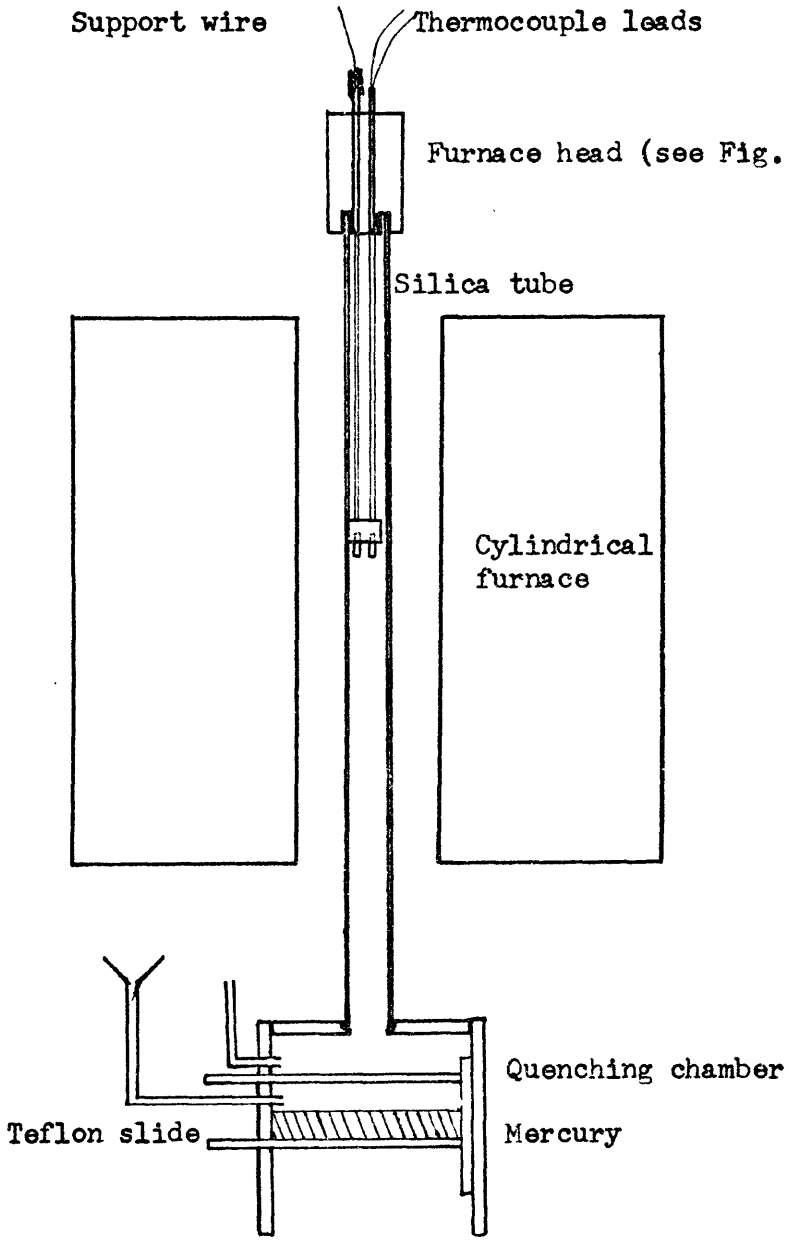


Figure 3 Schematic diagram of quenching furnace

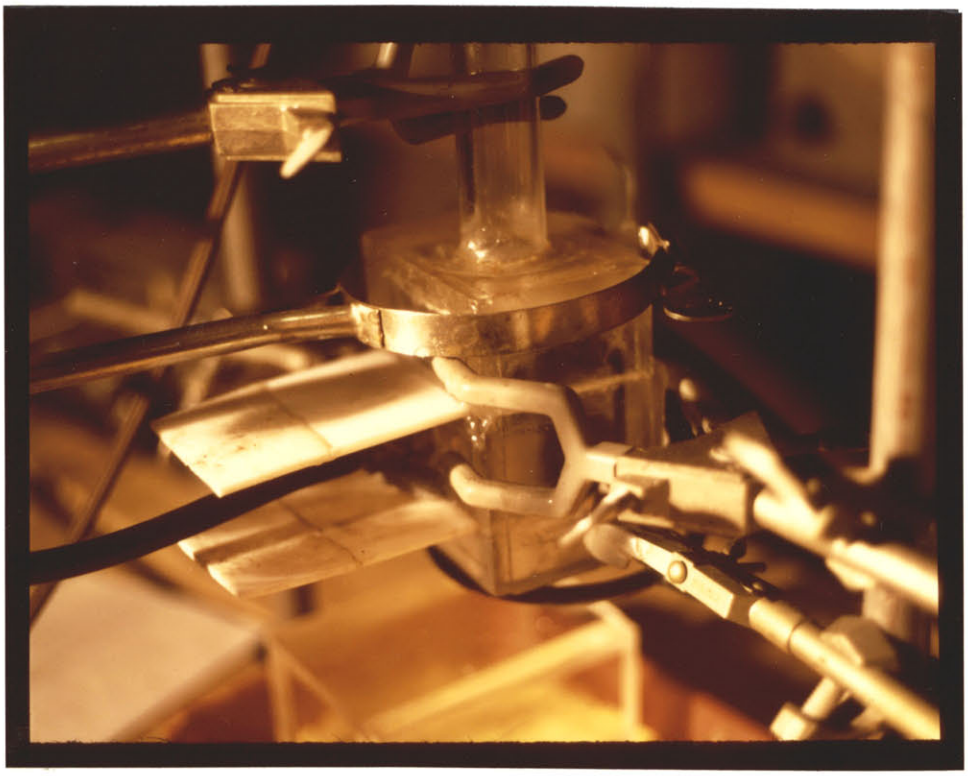


Figure 4 Gas inlet system. White plastic gastight slides visible at left. Furnace tube is held in upper clamp.

fluid. Problems which developed after construction showed that liquid nitrogen could not be used, however, because it would not flow freely enough through the inlet system into the quenching chamber under the influence of gravity alone, so the liquid nitrogen technique was abandoned. The system proved to be quite suitable for use with mercury, however, so that was used as quenching fluid. An enlarged fluid inlet might allow nitrogen to be used. The mercury was kindly provided by Professor P.M. Hurley.

Figure 4 is a photograph of the quenching chamber. It is an inverted open box of Plexiglas with a rabbeted hole in the top for the furnace tube. Two slots were cut into the box horizontally, into which were fitted Teflon sheets, so that they slid in and out like drawers. The sheets were long enough to protrude from one side of the box and fit into the slots in the side. They were supported at the edges by slots in the side walls of the box, and butted (when slid all the way in) against a piece of foam rubber glued to the rear wall of the box. When in place and properly covered with high vacuum grease (silicone type), they were perfectly gas tight. The gas mixture was introduced through a joint in the section of the box above both slides. If either was closed, the gas flowed freely through the upper part of the box, out the top hole, and into the furnace tube. Between the two slides was a connection through which mercury was introduced by means of a funnel and flexible tube with pinchcock. If the bottom slide was closed, the mercury collected on the bottom plate.

In operation, mercury was allowed to flow into the chamber with the bottom slide closed until it was half filled, then the mercury supply cut off at the pinchcock. The top slide was pulled out part way, so that the surface of the mercury was exposed to the furnace opening. A sample being quenched dropped in its capsule into the mercury. During all this time, the system was still gas tight because the upper plate sealed the opening to the air, as did the bottom plate. When the sample was in the mercury (floating on it), the top plate was slid all the way in, isolating the middle chamber from the gas stream. Then the bottom plate was slid out and the mercury and sample fell into a plastic cup placed under the apparatus. Care was taken to catch all the droplets of mercury, which almost always splashed to some extent. The bottom plate was then closed and fresh mercury introduced into the middle chamber in preparation for the next quench. Mercury vapors produced by the quench flowed up through the furnace with the gas mixture and were ported with the already toxic gas mix directly into the fume hood vent. The apparatus was checked from time to time for the presence of toxic mercury vapors, and any spilled mercury was cleaned up immediately. A tray of powdered sulfur below the apparatus provided a surface to collect mercury droplets and also combine with mercury vapor and lower its concentration in the surrounding air. After the sample was removed from the mercury, it was reintroduced into the funnel and recycled through the system. Any contamination of the mercury by particulate matter, such as sample crystals leaked from a cap-

sule, was removed by filtering the mercury through standard filter paper with a pinhole put through the tip, allowing the mercury to flow out. This also provided a convenient way to remove sample capsules from the mercury.

Thus, throughout the entire quench cycle, only an insignificant amount of air (that contained in the volume between the two plates) was allowed into the system, and that is flushed out very quickly. Samples were quenched separately, and at any time, the length of the run being limited only by the quantity of gases available. With a multiple tank connection manifold, runs could last for extended periods of time.

Samples were contained in platinum capsules made from 3 mm platinum tubes, 1 inch long, open slightly to the furnace atmosphere. At very high temperatures, approaching melting, significant amounts of iron may be lost into the platinum, but at 1000°C or less, the losses should be insignificant. Other capsule materials may be used, but the high return value of platinum (which could even be reused for experiments where no melting takes place) makes it the material most convenient and economical. Silica tubes could also be used if a suitable method can be devised for hanging them on wires, which is the method used to support the capsules.

Capsules were crimped shut at the bottom, filled with sample, then crimped onto a fine platinum wire by which they were hung in the furnace. The top crimp extended only part way across the opening so that the furnace gases could enter freely and equilibrate with the sample. The

capsules were hung by these wires in a position predetermined to be the hot spot of the furnace.

The capsules and wires were kept from touching each other at high temperatures because of the possibility of entangling or actual welding of the parts. This was accomplished first of all by a spacer, (Figure 5) cylindrical in shape, which has cavities in its lower surface into which the capsules were drawn. A smaller hole extended from the top of the cavity through to the upper side, through which the support wire was fed. The spacer was made of Lava "A", a product of the American Lava Corp. which may be readily machined into the required shape, then fired to drive off water and make it strong and stable. Because it is nearly pure Al_2O_3 after firing, it was assumed to have little effect on the samples because of its extremely low vapor pressure. Above the spacer, the wires were sheathed in silica thermocouple tubing to prevent their touching.

The spacer had seven identical cavities (although it could possibly be designed to have more or less) into which capsules could be placed, arranged in a circle. The eighth hole was in a similar position but was enlarged to accomodate a thermocouple, which was constructed so that the junction was in the same position as the middle of a capsule. The two thermocouple wires (which were chromel and alumel in the present study, but could be platinum and platinum-rhodium for higher temperatures) were separated by a small ceramic bead so that there was no electrical junction where they passed through the spacer. Above that, they were

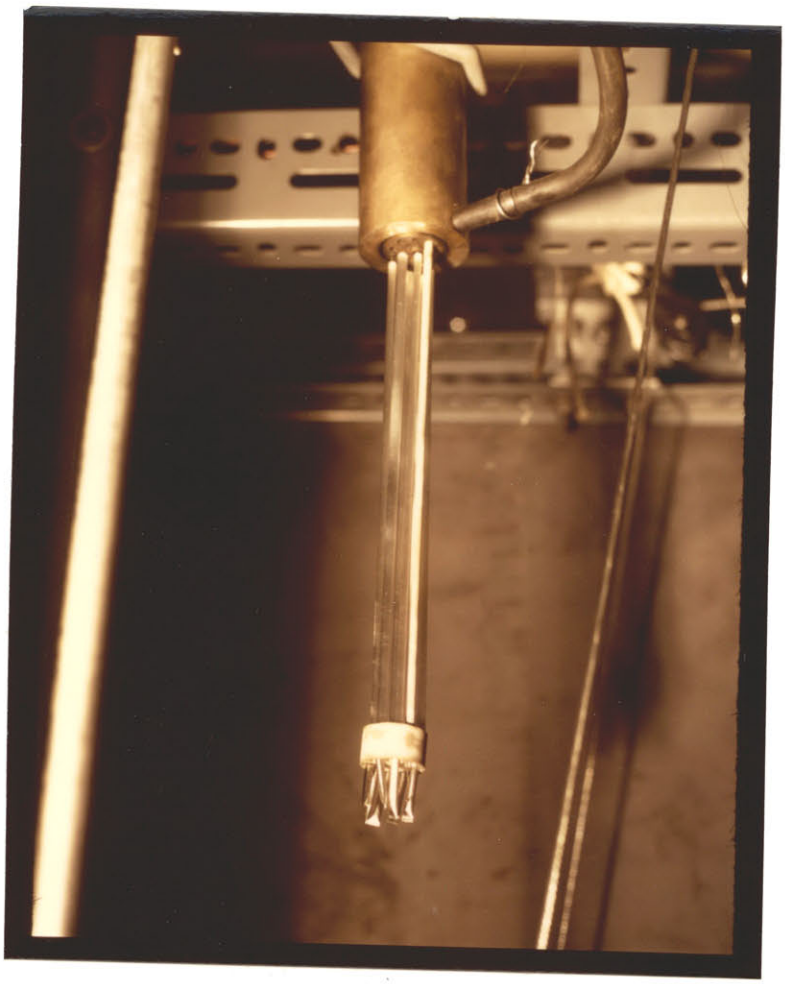


Figure 5 Spacer with sample capsules ready to go into the furnace. Bottom of furnace head joint appears at top. Between are support and thermocouple wires with silica and ceramic sheathing tubes.

contained in two-hole ceramic thermocouple tubing, which extended all the way up through the top joint of the furnace to the air, where they were connected to a current measuring system.

The top joint of the furnace was designed to be impervious to very hot gas, which passed into it continually from the furnace. In addition, it had feed-through holes for the various support wires and thermocouple wires, and a channel through which the gas mixture could flow, be cooled, and vented into the fume hood. It sealed tightly on the furnace tube, just as the bottom joint, to prevent air leaks.

Cooling water circulated through the brass head (Figure 6), which capped the furnace. The top of the furnace tube fitted into a cavity in the head and sealed with an "o" ring and vacuum grease. The wires for support and the thermocouple were inserted through tubes of brass which extend all the way through the head. The head is hollow, and cooling water is circulated to cool the wires and gas in the brass tubes. The tubes protruded from the top of the head, and has a short length of rubber tubing slipped over them. The wire came up through the tube, through the rubber tubing, and out into the air. The rubber tubing acted as a seal when pinched shut with a screw clamp, which also held the wire in place. The tubes through the head were arranged in a pattern identical to the holes in the spacer, except that one extra tube was provided in the very center through which the gas mix was vented. It was cool enough after passing through the head to be vented from there with ordinary Tygon or rubber tubing.

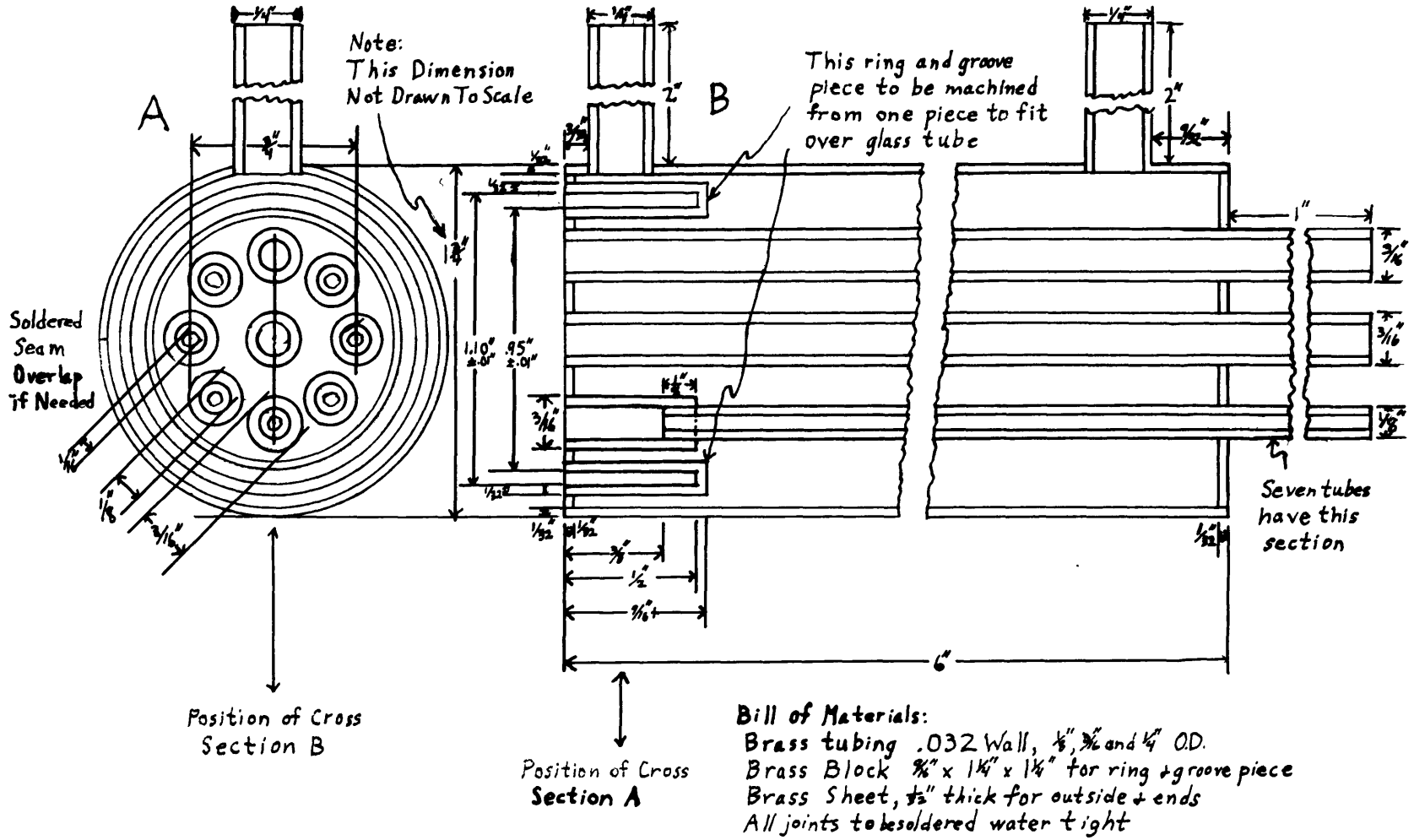


Figure 6 Head joint for furnace.
To fit over silica tube.

The spacer was attached firmly to the thermocouple by slipping it down until it wedged against the ceramic bead. The spacer could then be raised or lowered by simply raising or lowering the thermocouple tube, which protruded above the top of the head. In addition, however, the silica thermocouple tubes which sheath the sample support wires were cut to exactly the correct length between the head and the spacer, maintaining it at exactly the correct spot in the furnace. This spot was predetermined during the calibration of the furnace. When the samples were drawn up tightly to the spacer, the whole system was fairly rigid and could be slipped down onto the furnace tube fairly readily and clamped into place. The assembled head, with samples, is pictured in Figure 5.

To make a furnace run, the gas mixer was started well ahead of time in order for the oil in the mixer to become saturated with gas and the flow rates to attain calibrated values. The furnace system was assembled and checked for leaks by pinching off the exit tubing momentarily to see if the pressure in the gas mixer manometers dropped. Leaks were stopped with vacuum grease, which has a very low vapor pressure at room temperature and should not have affected the samples, especially since the system was being flushed with gas continually. Then the cooling water was turned on and the furnace started.

Temperature inside the furnace was monitored by the thermocouple, which was calibrated against the melting point of gold and of sodium chloride. This was done inside the furnace in the same position as the thermocouple was to take during an actual run.

Temperature control of the furnace, however, was accomplished with a probe inserted between the silica tube and the ceramic furnace tube, connected to a commercial proportional temperature controller. The setting on the controller, of course, did not correspond to the thermocouple in the gas stream, but once set did provide good long term stability of the temperature inside the tube. In a permanent setup, the controller probe must be mounted so that it does not move. Experience with the furnace built for this study showed that a controlled reproducible temperature could be reached, even after the furnace was shut off, dissembled, reloaded, reassembled, the controller turned on again.

The hot spot of the furnace was determined with the gas flowing at the same rate as during the experiments. The hottest zone was about 2 cm long with a maximum variation of only about $\pm$ 2°C through the zone. The hot spot moved only about 6 mm when the gas flow was stopped.

Temperature readout of the thermocouple was monitored with a Leeds and Northrup potentiometer, which was calibrated to read out in millivolts the EMF of the thermocouple relative to the EMF of a thermocouple immersed in an ice bath. Temperatures were read from tables provided by Omega, Inc., and were a compilation of the most recent values of thermal EMF for various thermocouple combinations. The values for temperature were corrected in accordance with the melting point determinations of gold and sodium chloride. A more convenient setup for temperature readout would involve a modern digital thermometer, which

would also result in reduced cost.

Runs used .150 gm of orthopyroxene, which was previously crushed (maintaining iron free conditions) and sieved to obtain the size fraction between 35 and 42 mesh (~.40 mm). This was placed in the capsule made by crimping one end of the platinum tube, then crimped onto the wire (which was already threaded through all spacers and the head of the furnace). The bottom spacer was supported in place by the thermocouple as noted above. Samples were drawn up into the cavity in the spacer until all were in place, then the head was lowered onto the top of the furnace tube, sealed in place, and the system checked for leaks. The temperature controller was set to the approximate value desired, and started.

Temperature runup lasted as long as about 45 minutes at 800°C. It was assumed (and later verified) that very little change took place in the degree of order in a sample until a temperature of about 750°C was exceeded, at least in a time scale of minutes. Heating above that temperature of course did start further disordering in the sample, so the final temperature was achieved as quickly as possible. The first sample was quenched immediately on reaching the final run temperature, in order to evalute any changes that might have taken place.

A second way of correcting for runup time changes in the sample was to change the method of operation slightly. A single capsule with sample was crimped onto the end of a long wire which had been threaded through the furnace head and the spacers. The sample, instead of being

drawn up into the cavity in the lower spacer, was allowed to hang all the way down into the quenching area of the furnace. After the temperature had stabilized at the desired value, the sample was drawn up into the proper position, held there for the desired length of time (usually a few minutes), and then quenched.

Quenching of either type of run was accomplished by simply unclamping the wire at the top connection to the furnace head and pulling firmly. The sample capsule would then break free from the wire, or the wire would slip out of the crimp, and the capsule would fall directly down into the mercury below. The stiffness of the spacers permitted this without disturbing the other samples in the run. This proved a very satisfactory arrangement. It was simple, economical, and reliable. Only the weight of the sample and capsule was supported by the wire, the spacers being supported by the thermocouple, so that accidental release of samples was very infrequent.

The furnace proved to give reliable and simple service after construction, despite the fact that it was built with economy in mind. Several of the design features proved very helpful in rapid processing of samples. Quenching of a sample required only a few minutes for the process including a temperature check. During the remaining run time, no maintenance was required except periodic checks to make sure the gas mixer received adequate supplies of gas to insure overflow, and temperature checks. The latter may be accomplished with a chart recorder if desired. Another possible improvement in the apparatus would be to place

an oxygen fugacity sensor probe in a sample position, and record continuously the current flowing through it (Sato, 1971). In this way, complete records of the operation of the furnace could be kept.

Chapter 3 MOSSBAUER SPECTRUM METHODOLOGY

Since its discovery in 1958, the Mossbauer effect (recoilless nuclear gamma ray emission and absorption) has proven a valuable technique in physics and chemistry, and more recently in geochemistry. The Mossbauer effect was used in this study as a tool to determine the relative ferrous iron populations of the two similar but not identical crystallographic sites in the orthopyroxene structure. Gamma rays were emitted from an excited state of iron 57 which was produced by decay from a prepared source of cobalt 57. A certain percentage of the gamma rays emitted resulted in no excitation of vibration in the lattice of the source, and so were emitted with an energy defined precisely by the energy of the nuclear transition itself. This energy was modulated by a Doppler shift, utilizing simple mechanical motion of the source vibrating toward or away from the absorber. In a similar fashion, radiation was resonantly absorbed by iron 57, a component isotope of natural iron. A resonant absorption takes place in iron atoms in minerals if the energy of the incoming gamma ray is precisely matched to the energy of the absorbing nucleus. The small energy difference made by the crystalline environment can be compensated for by the Doppler shift induced by the vibrator. When a range of velocities is scanned, the spectrum produced has separate absorption peaks for each iron site. If the peaks do not overlap greatly, the spectrum can be decomposed into its component peaks, and, in favorable circumstances, the areas of the

peaks will be a measure of the number of iron atoms in each coordination site.

There are two crystallographic sites for the ferrous iron in orthopyroxenes, each giving rise to a doublet absorption peak, or a total of four peaks. These are imperfectly resolved at room temperature, but resolution is much improved at 77°K. The sample also must be powdered and the orientation of grains randomized in order to eliminate asymmetry in the size of the two peaks of each doublet, which could cause problems for the curve fitting routine used to analyze the data, and also give incorrect results.

The major consideration in these experiments was to obtain very high precision in the measurement of peak areas, as well as high accuracy. With homogeneous sample splits, differing only by their heat treatment and reaction with the buffering gas mixture, it was hoped that other effects would be cancelled out. The spectrometer, an Austin Science Associates, S3, K3, was set up in the same configuration and samples run at identical temperatures each time. The data were accumulated in a multichannel analyzer with 512 channels, about .008mm/channel, which is more than adequate for resolving any peaks that can be resolved using present techniques. All equipment adjustments were made carefully and then not changed for the duration of the runs. An oscilloscope was used regularly to check on the operation of the equipment, especially the drive signal feedback, which is the best indication on the spectrometer that the equipment is working properly. Room temperature was main-

tained at a constant value as carefully as possible in order to stabilize the drive electronics.

A special table was devised working on the principle of the inverted pendulum and tuned to a very low frequency. It was designed to hold the Mossbauer source drive, the detectors, and associated cryostats and high pressure equipment, linking them rigidly together but insulating them from spurious building vibrations which could affect the drive, especially in the low velocity regions which lie under some of the peaks in orthopyroxenes. The principle was derived from a device supplied by Austin Science Associates to insulate the drive and detector for small samples.

This table is shown diagrammatically in Figure 7. A rigid table, of 3/4" plywood, was built around a steel pipe frame. A platform, also of 3/4" plywood, was provided at a convenient distance below the table top, to hold 25 liter flasks of liquid nitrogen for the cryostat. The top of the table holds the Mossbauer drive, detectors, and high pressure systems. The shelf is in turn supported from underneath by two specially designed feet which run from front to back of the table. The feet are spring steel sheets, about 4" wide and run from front to back of the table. They are clamped along the top edge to the shelf of the table, and along the bottom edge to wooden blocks. The center, about 2", is free to bend from side to side. Weight is added to the table until it oscillates very slowly when pushed sideways and released. This tuning of the oscillation then makes an effective mechanical damping system for

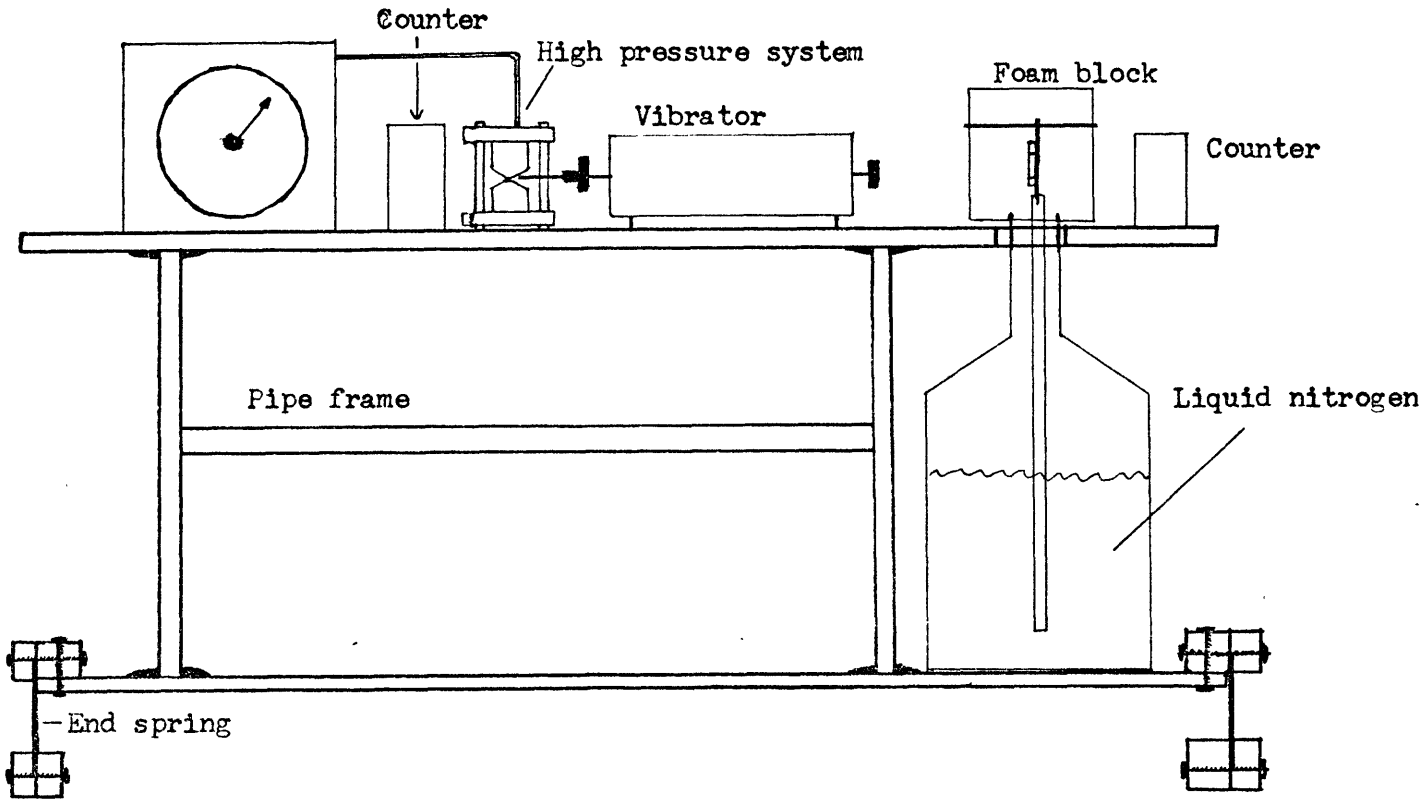


Figure 7 Mossbauer spectrometer support table

any vibrations of low frequency transmitted through the floor, and will help prevent vibration transmission from the air. Large wedges were constructed to hold the table steady while changing cryostat flasks.

Some previous difficulties with peak intensities in the low velocity region were improved after installation of the system. Having the entire system linked solidly together also made alignment and adjustment easier, both for high pressure and for low temperature work.

Samples were weighed before being placed in the furnace, and all were .150 $\pm$ .002 gm. After quenching, the samples were removed from the capsules directly into a mortar, covered with acetone to prevent oxidation, and ground thoroughly by hand. Sugar was then added in about an equal amount, and the two ground together momentarily. When the acetone had evaporated, the sample was transferred to a sample holder which consisted of a Plexiglas sheet with a hole 2.2 cm in diameter cut in it. The windows for the transmission of the gamma rays were transparent tape, which also held the sample in place. The sample was not compressed but packed loosely so as to minimize any preferred orientation. (See Appendix 2 for a discussion of peak intensity and preferred orientation.) For runs made at the temperature of liquid nitrogen, the sample was taped to a copper plate which had a hole just large enough to mask the holder but not the sample. This copper plate was connected to a copper rod which hung down into a 25 liter tank of liquid nitrogen. Styrofoam was pushed down over the top of the copper sheet and held in place by a dowel passing through the styrofoam and through a hole in the

copper plate. This thermally insulated the sample. The neck of the nitrogen tank was sealed to the styrofoam with a ring of flexible closed cell foam. To ensure a tight fit, a lead plate was placed on top of the styrofoam to hold it firmly down onto the nitrogen tank. The sample was then aligned with marks on the styrofoam, and finally by use of a ratemeter on the output of the proportional counter. All of the experiments were run with one source, cobalt 57 in palladium. The number of counts used for each sample varied, but most were about 600,000 counts per channel, with some as low as 400,000. Each of these figures is quite large, and no great increase in precision could be achieved by increasing the count rate by any reasonable amount. Use of a moderately active source (50 mCi) helped limit the time duration of a run and thus minimize drift of the electronics.

The spectra were read out in digital form and processed with the computer program of A.J.Stone, as modified by F.E.Huggins. This fits the known theoretical Lorentzian line shapes to the data, one Lorentzian to each peak specified, with initial constraints on parameters for economy in fitting time, constraints which may be removed selectively as the fitting routine progresses. Initial estimates of spectrum parameters must be provided to the program. In order to minimize program induced variation, the same initial estimates, established by carefully fitting one of the spectra obtained, were used for each of the spectra fitted.

The first group of samples run were not heat treated, but simply

splits of the original sample mix. They were treated in exactly the same way as the others in order to establish the precision of the system. It was thought that these would be the best test of the system because the metamorphic origin of the sample indicated that the iron occupancy of the M1 site would be quite low, and this relatively small peak would be the most difficult test of the equipment to correctly resolve it from the much larger M2 peak and accurately obtain its area. This was especially true in the low velocity region where the lower energy peaks of the doublets occur fairly close together. All other samples should be identical except that the area of the M1 peak would be increased, resulting in even better data.

There is some controversy over the use of line width constraints in fitting spectra. There is at present no theoretical justification for constraining the widths to be equal for all ferrous peaks, but this procedure is widely used. The main justification is that the widths should be equal if the sites being fit are identical, all lines are Lorentzian in shape, and the samples are relatively thin. Because most octahedral sites in minerals are similar in size and shape, they are observed to have quite similar line widths in many experiments; it is assumed that they may actually be more nearly equal than the program fits them. As Dowty and Lindsley (1973) point out, possible relaxation effects at low temperatures make this a dangerous assumption, especially for low Fe pyroxenes. All spectra were fitted both with and without width constraints. The spectra without width constraints showed a

greater variation in peak areas, even for the same samples, most of which could be correlated with variation in the linewidths. Higher precision was obtained by constraining widths to be equal. However, since the theory developed in later sections makes it necessary to obtain absolute site populations, unconstrained width data were used. This procedure also allows direct comparison to be made with the data of Saxena and Ghose (1971).

Six spectra were taken of sample HCo, and all were well resolved into four peaks. With widths unconstrained, the areas were expressed both as absolute values and as a percent of the total resonant absorption. When the values of percent absorption for the two peaks of the M1 doublet are added, the result is the percent of total iron that is in the M1 site, assuming that the recoil free fraction, f, is the same for each site. This assumption has been justified fairly well by the work of Dowty and Lindsley (1973), and Virgo and Hafner (1969), on the Mossbauer spectrum of ferrosilite, and also by the similarity in temperature factors obtained in x-ray diffraction studies. Spectral data are given in Table 3. The final fraction of the total iron in $M1_A^{T(M1)}$ was found to be .102. The standard deviation for the six runs was .00345 or about 3.5% of the value. One of the numbers making up this mean was taken from a spectrum run fairly late in the series of experiments, and did not differ significantly from the others. The absolute value of the standard deviation is probably the most significant measure of the error, because in cases where the M1 occupancy by iron is higher,

Table 3
Disordering Data

Sample Number	T°C temp.	Time of run, min.	Adj. time	Peak widths, mm/sec				T(M1)	X(FeM1)	log fO_2
M1	none	no heating for #1-5.		.286	.372	.404	.267	.1003	.0263	
M2				.306	.341	.391	.219	.1039	.0273	
M3				.284	.340	.386	.251	.1024	.0269	
M4				.311	.348	.400	.234	.0982	.0258	
M4(dup)				.332	.340	.388	.238	.1078	.0283	
M5				.294	.345	.394	.276	.0998	.0262	
M13	1000	?		.321	.300	.315	.291	.2899	.0762	-16.0
M14	1000	?		.358	.329	.324	.334	.2902	.0764	-16.0
M15	1000	?		.306	.305	.316	.280	.2970	.0780	-16.0
M16	1000	?		.328	.309	.330	.273	.2960	.0778	-16.0
M19	1000	?		.364	.336	.345	.299	.2983	.0783	-16.0
M20	800	44	6	.322	.351	.398	.266	.2638	.0692	-19.8
M21	800	120	82	.370	.379	.409	.303	.2933	.0770	-19.8
M22	800	198	160	.324	.357	.411	.247	.2840	.0745	-19.8
M23	800	280	242	.318	.339	.384	.265	.2864	.0752	-19.8
M24	800	608	570	.310	.357	.401	.256	.2625	.0689	-19.8
M25	800	1353	1315	.344	.358	.396	.271	.2753	.0722	-19.8
M26	800	2186	2148	.308	.378	.400	.272	.2589	.0679	-19.8
M27	600	32		.322	.381	.407	.305	.0962	.0252	-24.0*
M28	600	89		.270	.354	.382	.238	.1004	.0263	-24.0*
M29	600	156		.288	.359	.400	.229	.0972	.0255	-24.0*
M30	600	216		.304	.354	.394	.224	.0990	.0260	-24.0*
M31	600	571		.343	.356	.392	.249	.1227	.0322	-24.0*
M32	600	847		.304	.372	.388	.286	.1119	.0294	-24.0*
M33	600	1386		.324	.346	.385	.215	.1369	.0360	-24.0*
M34	800	12	12	.324	.341	.387	.251	.2744	.0720	-19.8
M35	800	5	5	.332	.345	.401	.242	.2418	.0634	-19.8
M36	800	20	20	.338	.339	.393	.274	.2816	.0739	-19.8
M37	700	31.5		.331	.341	.403	.205	.1091	.0286	-22.3
M38	700	55		.364	.397	.398	.267	.1550	.0407	-22.3
M39	700	145		.330	.343	.388	.266	.2040	.0535	-22.3
M40	700	350		.318	.345	.411	.256	.2157	.0565	-22.3
M41	700	1260		.386	.345	.412	.262	.2408	.0632	-22.3
M42	700	1545		.351	.348	.411	.259	.2349	.0616	-22.3
M43	700	4180		.337	.363	.444	.263	.2398	.0629	-22.3
M45	800	207	207	.304	.355	.403	.267	.2713	.0712	-19.8
M46	700	35		.283	.341	.396	.188	.1152	.0302	-21.1
M47	700	98		.306	.339	.410	.239	.2014	.0528	-21.1
M48	700	163		.359	.353	.394	.271	.2203	.0578	-21.1
M49	700	223		.312	.350	.407	.271	.2142	.0562	-21.1
M50	700	321		.336	.375	.429	.257	.2178	.0572	-21.1
M51	700	400		.319	.353	.425	.260	.2242	.0588	-21.1
M52	700	474		.308	.349	.427	.259	.2293	.0602	-21.1

Sample number	T°C temp.	Time of run, min.	Adj. time	Peak widths, mm/sec				T(M1)	X(FeM1)	log fO_2
M53	750	36.5		.375	.376	.433	.270	.1657	.0435	-21.0
M54	750	96.5		.331	.266	.407	.293	.2606	.0684	-21.0
M55	750	174		.339	.351	.404	.287	.2668	.0702	-21.0
M56	750	310		.358	.421	.423	.334	.2624	.0689	-21.0
M58	750	1830		.351	.349	.407	.280	.2722	.0714	-21.0
M59	750	8445		.308	.359	.403	.292	.2521	.0662	-21.0
M60**	700	34		.344	.370	.391	.230	.1114	.0292	-21.6*
M61**	700	199		.269	.367	.401	.241	.1840	.0483	-21.6*
M62**	700	379		.292	.336	.412	.266	.2115	.0555	-21.6*
M63**	700	495		.339	.344	.408	.278	.2312	.0607	-21.6*
M64**	700	655		.286	.342	.398	.242	.2119	.0556	-21.6*
M65**+	700	1375		.293	.350	.395	.252	.2017	.0529	-21.6*
M66**	700	2395		.336	.372	.405	.261	.2323	.0610	-21.6*

* Samples may not be buffered to these values. See text.
** Samples M60-66 were buffered with CO-CO_2, the rest with H_2-CO_2.
+ Sample M65 may be suspect due to problems during Mossbauer run.

the error of measurement should be proportionately less. Student's t test (Wallis and Roberts, 1956) gives 95% confidence limits of $\pm$ .0085 for unconstrained width data (cf. .007 for widths constrained to be equal).

One source of error in the measurements made is the area asymmetry that appears in the doublets. The lower velocity, lower energy, peak is consistently slightly larger than the other. There are several possible reasons for this, all or some of which may have contributed. One is the possible presence of unresolved ferric iron peaks, although Whipple (1973) has shown that ferric iron in orthopyroxenes tends to be low if the material is pure. One or two percent of the iron could be present as ferric ion and not show up as resolvable peaks. Other possible factors are preferred orientation of crystals which can produce pronounced asymmetry (see Appendix 2) and paramagnetic relaxation effects which could result in asymmetry in area and change of shape of the lower energy peak. It is of interest to note that the asymmetry changed during the heating experiments, possibly due to induced oxidation, broadening, or preferred orientation affecting one site whose iron occupancy changed. Two representative spectra, showing different degrees of ordering, are shown in Figure 8.

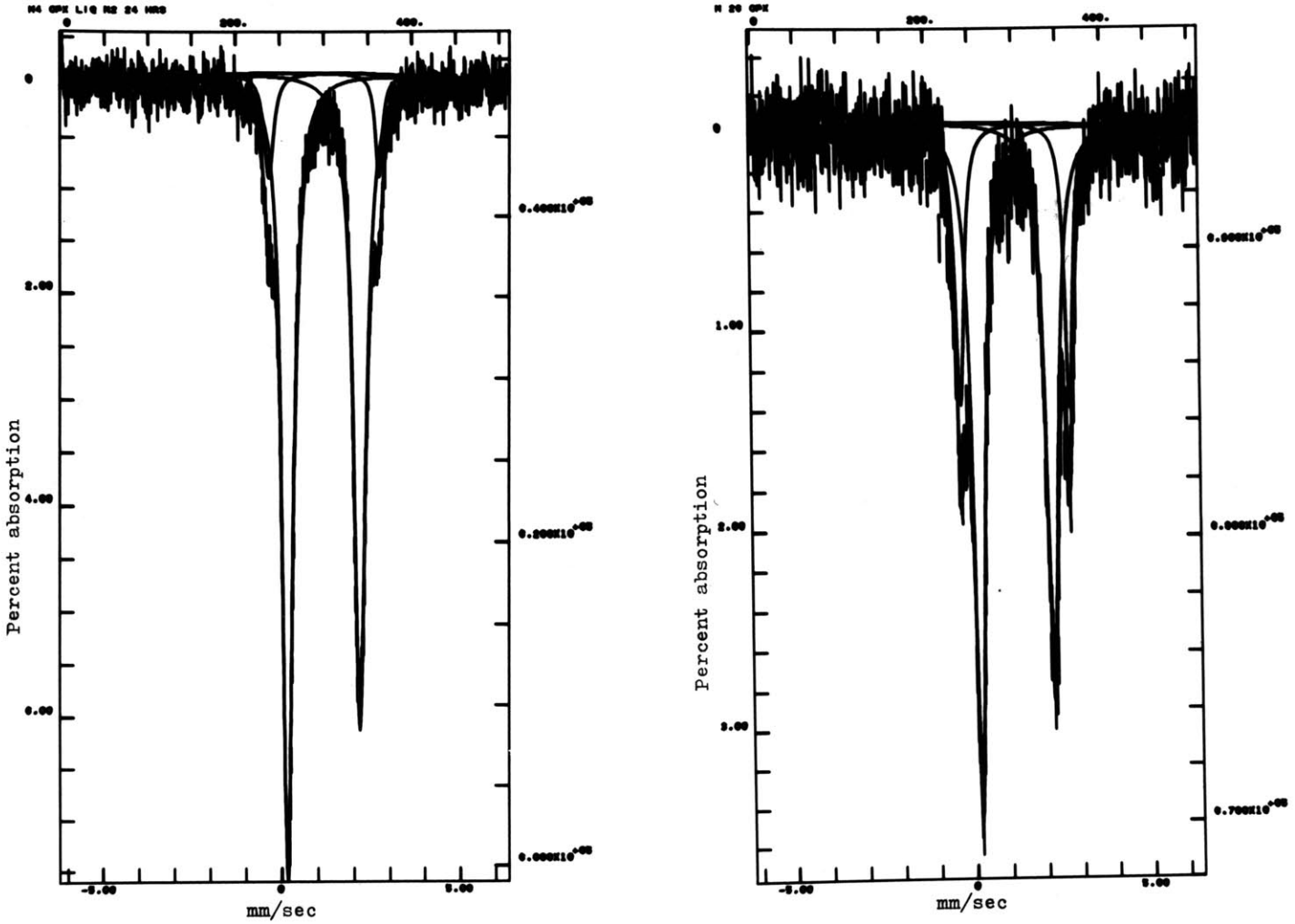
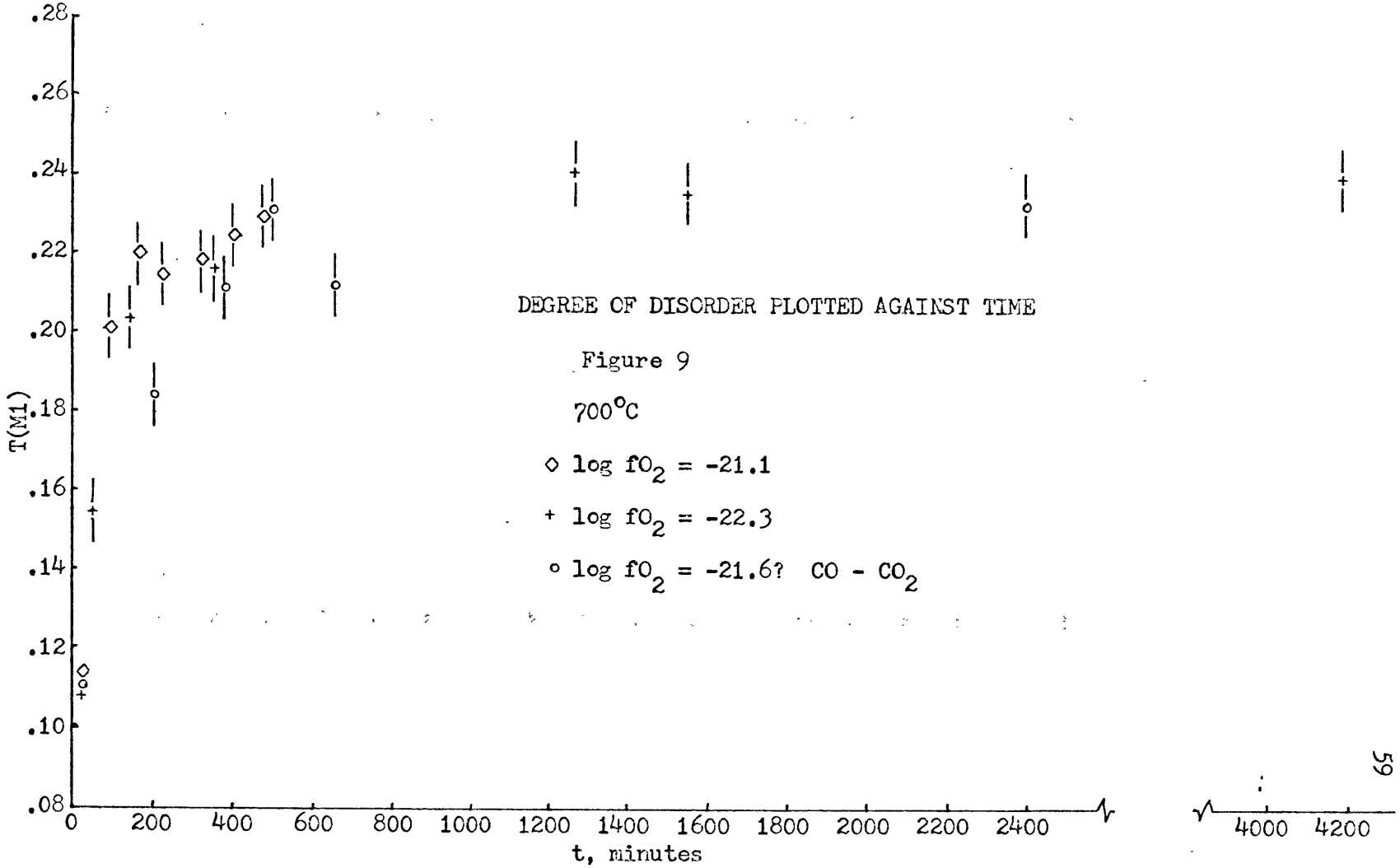


Figure 8 Representative Mossbauer spectra of sample HCo. Left-hand spectrum, natural sample. Right-hand, heated at 800°C.

Chapter 4 DISORDERING DATA

The data obtained in this study are shown in Table 3 and Figures 9 - 12. All experiments are for disordering reaction. Time did not permit a study of ordering experiments. The data are expressed as T(M1), the fraction of the total iron in site M1, determined directly from the Mossbauer data as the fraction of area under M1 peaks divided by the total resonant absorption area. This has been converted to atomic fraction in each site by multiplying by the factor 2Fe/ Fe + Mg = 2(.1312) on a six oxygen basis, for this sample as determined by electron microprobe analysis. Use of this factor ignores the presence of other cations such as Ca and Al, present only in minor amounts and having an unknown effect in any case. It was hoped that the site populations of these and other ions did not change significantly during experiments, but this cannot be proven.

The general trend of the data is toward increased disorder with time at any given temperature, as expected. Experimental difficulties were encountered with the support system in the first few runs, the wires being too thin to hold the weight of the samples and spacers, so that the data are incomplete and many samples were lost because the time of quench could not be determined accurately. With heavier wire and use of the thermocouple supporting system for the spacer, the apparatus became quite reliable and later sets of data comprise almost complete sets of seven samples.



DEGREE OF DISORDER PLOTTED AGAINST TIME

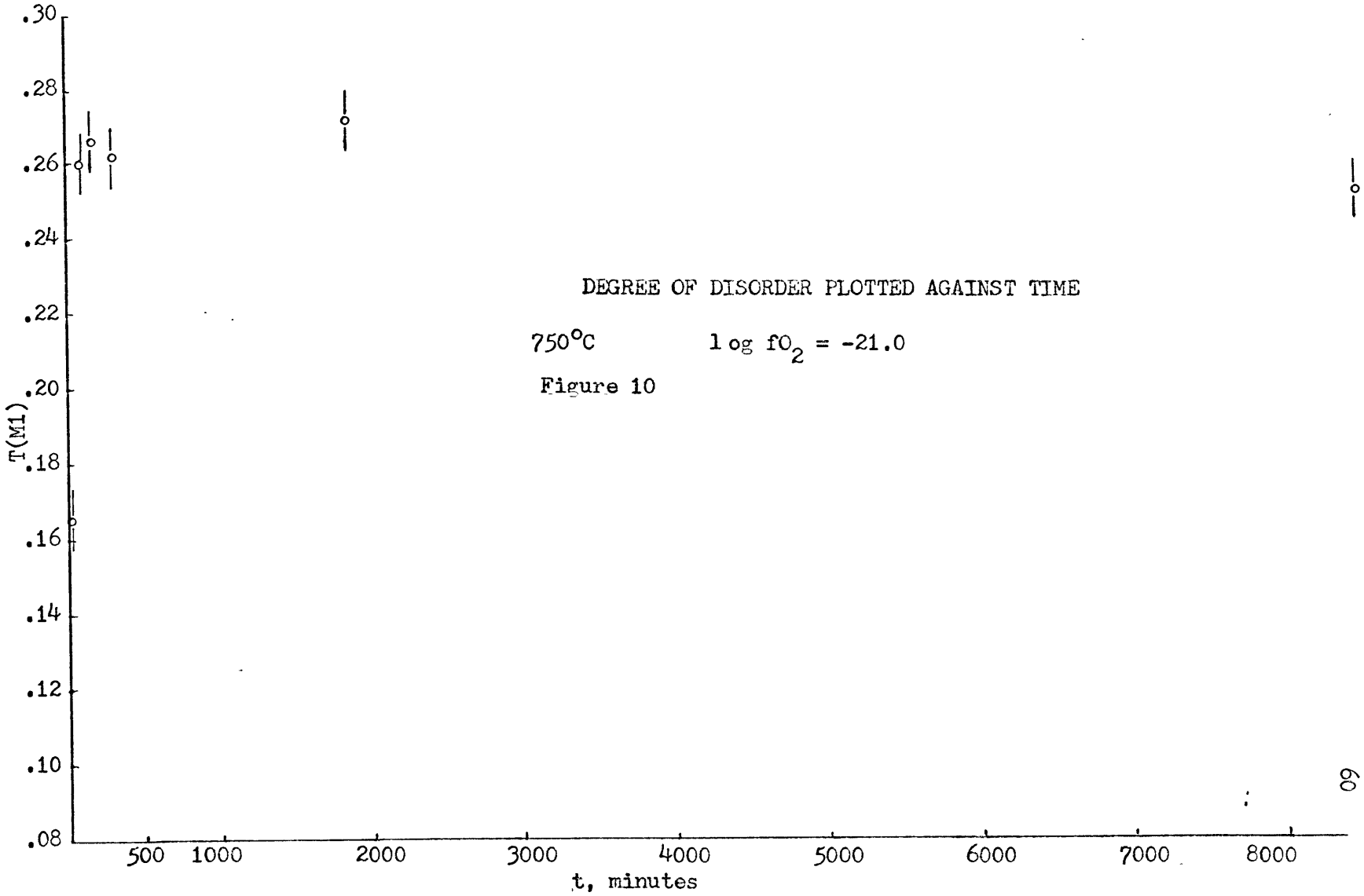
Figure 9

700°C

◇ log fO_2 = -21.1

\+ log fO_2 = -22.3

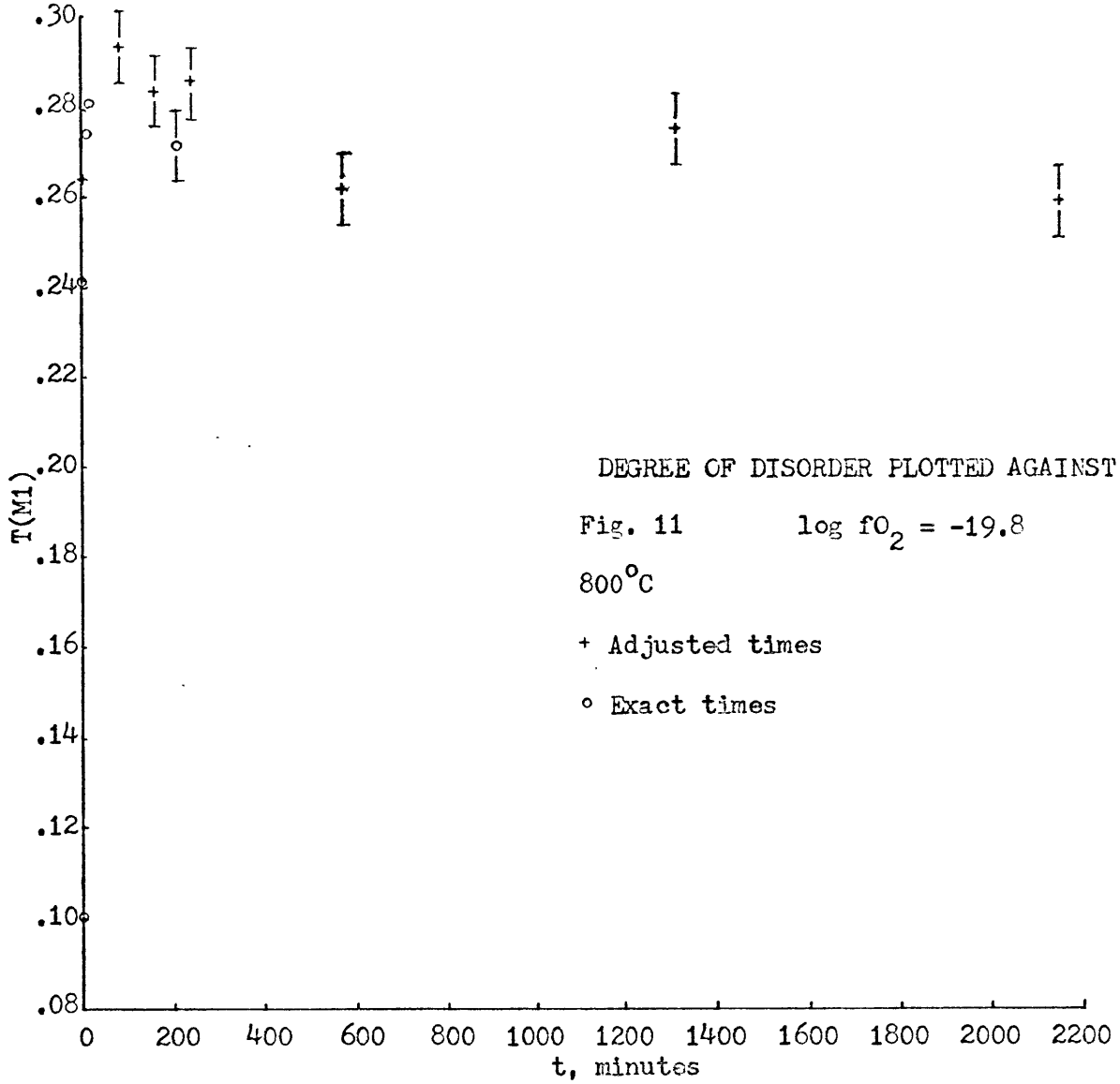
○ log fO_2 = -21.6? CO - CO_2



DEGREE OF DISORDER PLOTTED AGAINST TIME

750°C log fO_2 = -21.0

Figure 10



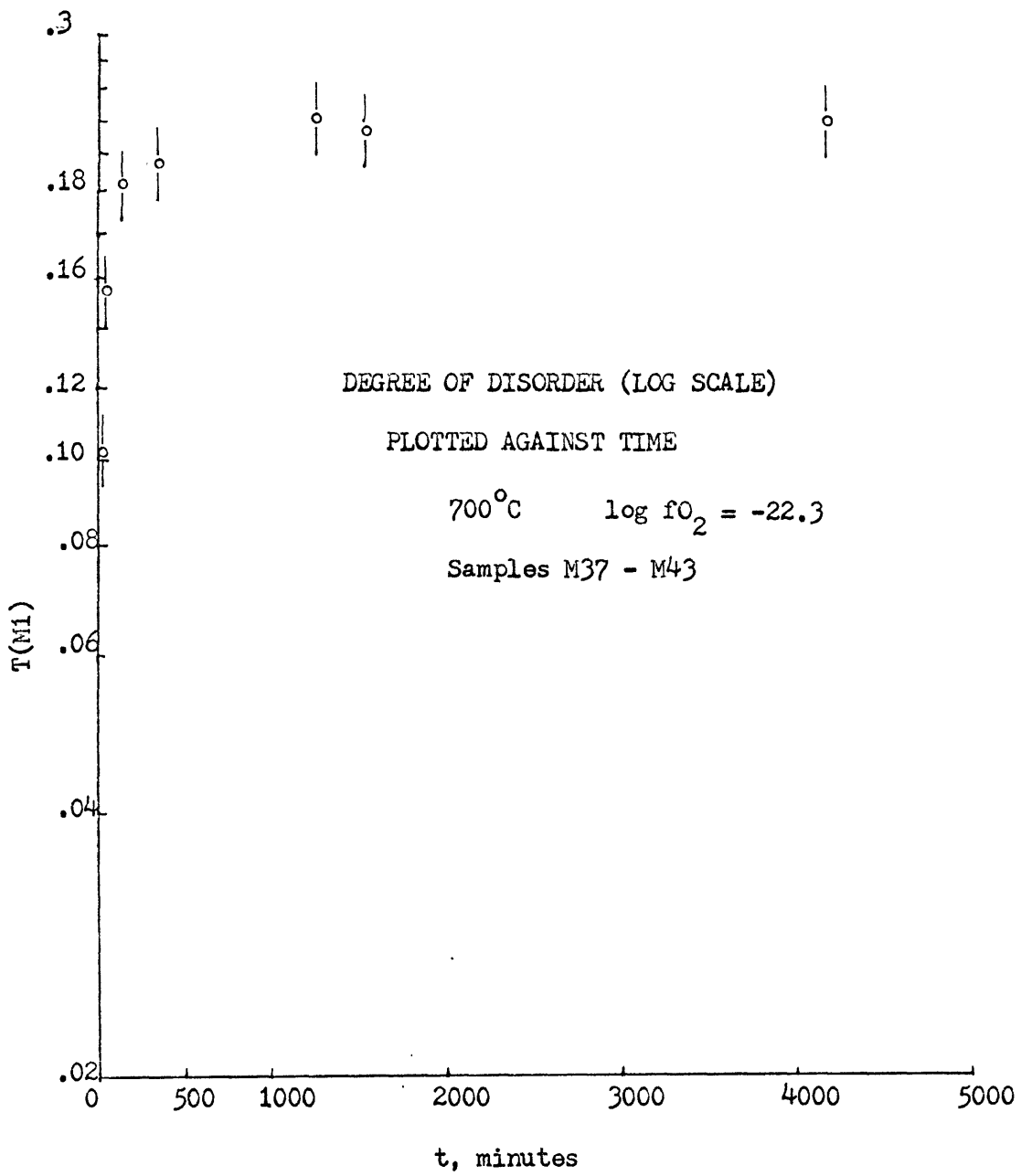
DEGREE OF DISORDER PLOTTED AGAINST TIME

Fig. 11 $\log fO_2 = -19.8$

800°C

+ Adjusted times

° Exact times


.3
.18
.16
.12
.10
.08
.06
.04
.02
T(M1)
DEGREE OF DISORDER (LOG SCALE)
PLOTTED AGAINST TIME
700°C
log fO2 = -22.3
Samples M37 - M43
0
500
1000
2000
3000
4000
5000
t, minutes

The first experiments were exploratory in nature, and of rather short duration. A temperature of 1000°C was chosen, since it was used for the marginal kinetic data of Virgo and Hafner (1969), who had indicated that complete equilibration was attained after only eleven hours, but measured almost no disequilibrium samples. The first experiment was terminated early because of the failure of the quenching apparatus to work properly, but some of the samples were run on the Mossbauer spectrometer (M13, M14, M15, M16, M19). The exact length of the experiment for some of these samples was not known (maximum times are shown), but the observed degree of order was much higher than expected for the relatively short times involved, and seem to have reached a T(M1) value of about .300, although some of the samples (which might have quenched prematurely) have somewhat lower values. The indication, at least for this sample, was that disordering times might be considerably faster than those of Virgo and Hafner.

The next experiment (samples M20-M26) was performed at 800°C, and $\log fO_2 = -19.8$, using H_2 and CO_2 as the buffering mixture. The gas mixing ratio was kept approximately constant for nearly all experiments. The graphical presentation of data by Muan and Osborn (1965, p. 52) showed that in the binary system iron - oxygen, single phase regions have almost constant stoichiometry for a given gas mixing ratio, regardless of temperature. Any minute variations in stoichiometry for the pyroxene, expressed as variations in the number of vacancies, would probably remain more constant at constant gas mixing ratio than at

constant fO_2. Any two-phase region for the iron - oxygen system has a constant value of fO_2 (at constant temperature) by the phase rule, but this is not the case for a single phase such as pyroxene.

Results for the first group of sample showed that the disordering increased with time, went through a maximum, then decreased slightly to a constant value. As this behavior was unexpected, duplicate runs with samples M44 and M45 were then made to verify the existence of the maximum. In addition, the relatively rapid rate of disordering, higher than expected, led to samples M34-36 being run. All of these experiments were performed by first bringing the furnace up to temperature, then raising the sample with the support wire until it rested firmly against the spacer. This provided rapid heating and a well defined starting time. In order to compare results of these experiments with multiple sample runs, an "adjusted time" was employed to approximate the effect of the heating time of the samples which were in the heated zone of the furnace during the time the temperature was being raised. An empirical figure of 38 minutes was used for runs at 800°C; this represents the length of time the furnace takes to reach approximately 750°C, the temperature at which relatively rapid disordering begins to take place. These 38 minutes were subtracted in the column marked "adjusted time" in Table 3. The adjustment factor will vary for different temperatures and different furnaces, and must be determined by careful temperature monitoring while heating the samples. For the lower temperatures investigated, this factor is (1) small and (2) not needed for comparisons; and thus ignored.

The first, and most surprising fact was the rapid disordering rate. The maximum change in disordering corresponded to T(M1) of .242, or almost complete disordering. In only 12 minutes, the value has reached .274, which is much higher than the final equilibrium value. Instead of maintaining a constant value for disorder, the amount of disordering gradually increases to a value of .293, then falls slowly to .259, its final equilibrium value. Possible explanations for this will be discussed later (Chapter 7).

At 600°C, the fO_2 of the gas mixture chosen was slightly within the calculated field of stability of graphite, the sample actually being buffered by the CO_2- H_2- C system and having a log fO_2 of about -24.0. These samples showed somewhat irregular progress toward disorder in 1400 minutes, and a much more sluggish reaction rate. Because of these considerations, no further experiments were done at this temperature, and the final equilibrium value of disorder for this temperature has not been determined. No falloff in rate of disordering with time is provable from the data obtained at this temperature.

With these two results, it became important to investigate some intermediate temperatures. A run at 700°C, with log fO_2 buffered to -22.3 by the same gas mixture as the above runs, proved to be intermediate in rate between the 600° and 800° runs. The time - disorder relation was unlike the 800°C run. Instead of reaching a maximum, followed by a slow falloff to a stable value, the disorder increased quickly at first, then more and more slowly, evidently not reaching

a true equilibrium value in almost 70 hours. The highest value reached, .240, is less than the disorder value for 800°, as expected, but is nevertheless surprisingly close.

Another run, at 750°C, was intermediate to the others: equilibrium T(M1) = .252, and intermediate in rate. There is a maximum as found in the 800°C data.

The log of the oxygen fugacity of the buffering gas mixture is given in Table 3. As noted above, all of these first samples were buffered with the same mixture of gases. To test the importance of the oxygen fugacity to the rate, the mixture was varied to a more oxidizing value for a run at 700°C, the most tractable experimental temperature. The resulting log fO_2 was -21.1, in contrast to the previous value of -22.3. This amount of alteration was conveniently made without having to change and recalibrate capillaries on the gas mixer. The data for the run showed a surprising amount of change, with the rate increasing. While the quality of the data did not allow a perfectly consistent factor of rate increase to be applied, some of the samples required less than half the time to achieve the same degree of disorder at lower fO_2.

Because hydrogen, a highly diffusable species, was present, a new run with CO-CO_2 as the gas buffering mixture was used to show the importance of fO_2 as the rate-changing factor. In this way, possible catalysis of bond-breaking by H_2, as discussed by Lacey (1965a, 1965b), could be eliminated. A log oxygen fugacity of -21.6 was chosen, inter-

mediate between the other runs at 700°C. A mistake in setting the gas produced a mix in the stability field of carbon, so it was assumed that the oxygen fugacity was that of the boundary of carbon stability. The mix may actually have been more reducing. Results were slightly slower than the run at log fO_2= -22.3 but not provably different. One sample, M64, is low in X_{FeM1}, perhaps due to experimental problems during the Mossbauer experiment.

A major problem was proving equilibrium within the gas mixture itself, and of the gas mixture with the sample. The oxygen fugacity of the gases was calibrated against the iron - wüstite reaction at 923°C. The gas mixture was changed slowly at constant temperature while four samples were withdrawn from the furnace. Microscopic examination proved the accuracy of the gas mixing system, for wüstite appeared on the iron wire at log fO_2 between -16.275 and -16.225, exactly on the reaction curve.

At lower temperatures, proof of equilibration of the gas mixture is more difficult. No attempt was made to determine the iron - wüstite reaction. However, rate changes of the disordering proved that the gases were changing the system. Because the changes in rate are in accordance with the predicted behavior for vacancy diffusion, the expected mechanism in most ionic solids, it is felt that the consistent direction of changes is a good indication that equilibrium is approached or reached. Arguments presented later (Chapters 6 and 7) do not in general depend on complete equilibrium of fO_2, as this is not <u>proved</u> in these experiments.

Chapter 5 DISCUSSION OF EQUILIBRIUM DISTRIBUTIONS

With the disordering data well established, an analysis of the energetics of disordering is possible at the temperatures investigated. As will be discussed later, the final data picked as equilibrium values are the results for the longest time of isothermal disordering. The maximum observed in the disordering curves is ignored.

The most comprehensive analysis of pyroxene order-disorder relationships is that of Saxena and Ghose (1971). They utilized a model for the orthopyroxene solid solution series, which represented the two sites as a simple mixture, and derived "activity" coefficients for each ion on each site to describe the nonideal nature of the solid solution. They determined isotherms utilizing data for heated pyroxenes of various compositions, and analyzed the data at each temperature with a least squares method to get interchange energies and true equilibrium coefficients from the distribution data.

The interchange of iron and magnesium between two sites is represented by:

(7) $Fe\ (M2) + Mg\ (M1) = Fe\ (M1) + Mg\ (M2)$

The equilibrium constant for this reaction is:

(8)
$$K = \frac{X^{o}_{FeM1}\ \gamma_{FeM1}\ X^{o}_{MgM2}\ \gamma_{MgM2}}{X^{o}_{FeM2}\ \gamma_{FeM2}\ X^{o}_{MgM1}\ \gamma_{MgM1}}$$

Where X^{o} is the mole fraction at equilibrium of the ion on the site

indicated, and γ the activity coefficient. Then the distribution isotherms may be represented by:

$$(9)\quad \ln K = \ln K_D + \frac{W_{M1}}{RT}(1-2X^{o}_{FeM1}) - \frac{W_{M2}}{RT}(1-2X^{o}_{FeM2})$$

where $K_D = X^{o}_{FeM1}(1-X^{o}_{FeM2}) \;/\; X^{o}_{FeM2}(1-X^{o}_{FeM1})$, X^{o}_{Fe} is the site occupancy, and W is the energy constant of the simple mixture model (Saxena and Ghose, 1971). The three unknown parameters, ln K, W_{M1}, and W_{M2} are found by a least squares fit of the data on site occupancy fractions obtained at one temperature for various compositions. The procedure used by Saxena (1973) is based on an iterative procedure, which is somewhat lengthy to program and use. A much simpler method is to use a direct computational form for least squares fit of data to three parameters. The method is outlined in Wallis and Roberts (1956). If the equation is written in the form $Y = a + b_1X_1 + b_2X_2$, ($RT \ln K_D = RT \ln K - W_{M1}(1-2X^{o}_{FeM1}) + W_{M2}(1 - 2X^{o}_{FeM2})$) first one calculates the mean of the three known variables, and the individual deviations from the means: $y = Y - \bar{Y}$, $x_1 = X_1 - \bar{X}_1$ and $x_2 = X_2 - \bar{X}_2$. Then

$$(10)\quad b_1 = \frac{\Sigma x_2^{\,2} \Sigma x_1 y - \Sigma x_1 x_2 \Sigma x_2 y}{\Sigma x_1^{\,2} \Sigma x_2^{\,2} - (\Sigma x_1 x_2)^2}$$

$$(11)\quad b_2 = \frac{\Sigma x_1^{\,2} \Sigma x_2 - \Sigma x_1 x_2 \Sigma x_1 y}{\Sigma x_1^{\,2} \Sigma x_2^{\,2} - (\Sigma x_1 x_2)^2}$$

$$(12)\quad a = \bar{Y} - b_1\bar{X}_1 - b_2\bar{X}_2 = \frac{\Sigma Y - b_1 \Sigma X_1 - b_2 \Sigma X_2}{n}$$

A shortcut to these computations is achieved by using formulas analogous to the following:

$$(13)\ \Sigma x_2^2 = \Sigma X_2^2 - \frac{(\Sigma X_2)^2}{n}$$

$$(14)\ \Sigma x_1 y = \Sigma X_1 Y - \frac{(\Sigma X_1)(\Sigma Y)}{n}$$

The resultant equation is that of a plane. Trial shows that this procedure gives the same result as that of Saxena and Ghose, when used with their data.

The lowest iron-bearing orthopyroxene used by Saxena and Ghose (1971) contained a Fe/Fe + Mg mole fraction of 0.181. Sample HCo used in this study has a corresponding mole fraction of 0.131, and therefore provides a new extension to previous data. Table 4 shows the results of calculations at 700°C and 800°C, both with and without sample HCo. W_{M2} is found to be the same at both temperatures for the new calculation, and W_{M1} is found to decrease only slightly with increase in temperature. The slight temperature dependence of the W's suggests that the excess entropy of mixing is almost zero, and that excess enthalpy of mixing is approximately equal to excess free energy of mixing. These results differ from the conclusions of Saxena and Ghose, who found significant excess entropy of mixing. The value of the distribution coefficient K_D for sample HCo shows that there is significant nonideality for high Mg pyroxenes as well as for high Fe pyroxenes, as it is higher than the

Table 4

Least Squares Fit of Distribution Data to Saxena-Ghose Model

973°K, without sample HCo

ln K= -1.29767 W_{M1}= 1916 cal/mole W_{M2}= 1215 cal/mole

973°K, with sample HCo

ln K= -1.04562 W_{M1}= 2334 cal/mole W_{M2}= 1974 cal/mole

1073°K, without sample HCo

ln K= -1.24133 W_{M1}= 1641 cal/mole W_{M2}= 1057 cal/mole

1073°K, with sample HCo

ln K= -0.981308 W_{M1}= 2217 cal/mole W_{M2}= 1989 cal/mole

values that would be extrapolated from the work of Saxena and Ghose (1971) on intermediate compositions. The value of ln K_D for 750° on HCo is intermediate between the 700° and 800° data, and would give approximately the same value of ΔG if the same activity coefficients are assumed.

From the values of ln K in Table 4, it is possible to calculate the free energy of the exchange: $\Delta G_{800°}$ = 2090 cal/mole, and $\Delta G_{700°}$ = 2010 cal/mole, which are in quite good agreement.

Further work on equilibria of low iron pyroxenes is desirable. Verification of the above results for another sample would be valuable and not overly difficult. Extension of the data to other temperatures would also be a useful experiment. A thorough understanding of the energetics of this relatively simple system will help interpret data from more complex systems.

Chapter 6 DEFECT EQUILIBRIUM AND DISORDERING

The principle factor controlling disordering rates is diffusion. It is only by movement of the cations through the relatively stable framework of the pyroxene structure that ordering and disordering can occur. There are essentially two forces at work, an energy term (enthalpy), which favors ordering of Fe into the M2 site, and entropy, which favors the most random distribution. At elevated temperatures, the entropy term becomes relatively more important, so that most disordering is favored by elevated temperatures. The algebraic sum of these terms, the Gibbs free energy, is an expression of the tendency for ordering or disordering. Diffusion must occur subject to the free energy differences.

The following discussion is adapted from the work of Flynn (1972). Traditional equations for diffusion are based on Fick's laws, which only concern concentrations of diffusion species, as do the disordering rate equations of Virgo and Hafner (1969), and Mueller (1967, 1969). However, these equations assume that no chemical change occurs. Fick's First Law is written

(15) $J_{\alpha} = -D_{\alpha} \nabla C_{\alpha}$

where J_{α} is the flux of species alpha, ∇C_{α} the gradient in its concentration, and D_{α} the diffusion tensor. If a chemical gradient is present, a somewhat different form is required, or a negative mixing rate would be predicted for processes such as exsolution. J is linked more funda-

mentally to the gradient in μ , the chemical potential, than to concentration. Then

(16) $J_\alpha = -C_\alpha M_\alpha \nabla \mu_\alpha$

where M is a mobility tensor, and is always positive in sign. The concentration term is added because the flux is proportional to the number of particles experiencing the gradient in chemical potential. Disordering may be thought of as interdiffusion between two interpenetrating systems, just as the distribution of cations was treated above as a distribution between two phases. Here the gradient in chemical potential is simply the difference in chemical potential between the present state of the system and the equilibrium state of the system. The rate of disordering would be proportional to the instantaneous difference in chemical potential, if all other factors were equal.

Another assumption must be made concerning the rate: both the mechanism and the proportion of diffusing defects must remain constant. Diffusion almost always occurs by movement of point defects in a crystal. Possible mechanisms are numerous: interstitial ions, vacancies, ring interchanges, crowdions, or even direct interchange of atoms. The only energetically favorable mechanisms in ionic solids are vacancy and interstitial motions.

The presence of some type of defect in minerals is inevitable. The basic reason is simple: the defects act as separate species in the crystal, and entropy considerations bar their total removal. The lower the number of defects, the more difficult is their removal. The presence

of a (ln x) term in entropy calculation explains the phenomenon: as x (mole fraction) approaches zero, the entropy term becomes infinitely large. For defects with relatively high energies of formation, their number is correspondingly low.

In silicates, the diffusion of silicon is much slower than the diffusion of cations of lower charge. Undoubtedly, this results from the relatively high energy requirements to form silicon vacancies, or interstitial silicon. The dominant diffusion mechanism is not known. Comparatively lower energy of Δ formation is probably the cause of the faster diffusion of divalent cations.

Fortunately, it is often possible to discover the relevant diffusing species in a given sample. Since energy of formation controls the number of defects of a given type, it is sometimes possible to alter the number by modifying the chemical potential in a crystal, through external buffering. For example, if the most common diffusing species is a cation vacancy, then lowering the chemical potential of the cation in the crystal (or raising the chemical potential of the anion) should result in an increase in the number of vacancies,and therefore an increase in rate of diffusion.

Vacancies may be stabilized by the presence of impurity cations of different charge. They will ordinarily be bound to the cation, and do little to influence the disordering rate. The major effect of the vacancies is to alter the diffusion rate of the impurity cations.

The number of various defects is greatly influenced by the charge

state of the crystal. A crystal in a buffering gas mixture will equilibrate with that mixture, and some charge transfer may occur. The maximum charge differential between a crystal and its surrounding vapor is not likely to exceed 10^9 excess charges per cm^3, or about 10^{-13} electrons per atom. Much of this may remain on the crystal surface, so that the charge imbalance is usually quite small inside the crystal.

Various species of defects interact. If an electron hole or anion vacancy is created, negative charge is removed from the lattice, leaving an excess positive charge. This modifies the lattice potential and a small excess of one type of vacancy modifies the formation energy of all other defects, thereby lowering the formation energy of oppositely charged defects. Near-equality of charged defect concentrations is assured (Flynn, 1972).

An extensive theory of the interaction of defects, using the charge neutrality principle, has been developed by Kroger (1964) and reviewed by Flynn (1972). The following discussion is derived from those sources, and represents the first mineralogic application of a comprehensive defect theory. If a crystal is always stoichiometric, the number of cation vacancies must equal the number of anion vacancies in order to conserve the number of sites. However, if very small deviations from stoichiometry are introduced, then charge balance can be achieved by a number of different equalities. The particular equation governing the imbalance in a given crystal depends of the potentials of the constituents.

The symbols used in this discussion are listed in Table 5, and follow the notation of Kroger (1964). The relations between various defect concentrations can then be formulated using mass balance and mass action principles. If the crystal is stoichiometric and equiatomic, then concentration of empty anion sites, $(V_X^{\cdot})$, is related to the concentration of empty cation sites, $(V_M^{'})$. The respective superscripts indicate positively and negatively charged defects with respect to the normal charge state of that site. Then,

(17) $(V_X^{\cdot})(V_M^{'}) = K_S^{'} = \exp(-g_s^{'}/2kT)$

by the law of mass action, where $K_S^{'}$ is the reaction constant, $g_s^{'}$ the free energy of formation of formation of the defect pair, and k the Boltzmann constant. Another equality of the same type is

(18) $(e^{'})(h^{\cdot}) = K_i = \exp(-g_i/kT)$

Because the vacancies are effectively charged, they can trap electrons and holes to form neutral vacancies. Further equilibrium conditions ensue:

(19) $V_M^X = V_M^{'} + h^{\cdot} + E_a$; $\dfrac{(V_M^{'})(h^{\cdot})}{(V_M^X)} = K_a$

(20) $V_X^X = V_X^{\cdot} + e^{'} + E_b$; $\dfrac{(V_X^{\cdot})(e^{'})}{(V_X^X)} = K_b$

It can then be shown that

(21) $(V_M^X)(V_X^X) = K_S^{'}K_i/K_aK_b = K_S$

where K_S is the reaction constant for neutral vacancies. Two equations describe equilibration of a crystal with its vapor:

Table 5
Notation for Defect Balance

Symbol	Meaning	
e	electron	
h	hole	
M	cation	
X	anion	
V	vacancy	
superscripts:		
'	negatively charged	with respect to the charge state of that site in the perfect crystal.
•	positively charged	
x	neutral	
subscripts:		
i	interstitial	
M	on a cation site	
X	on an anion site	

(22) $M(g) = M_M^X + V_X^X + H_M$

(23) $\frac{1}{2}X_2(g) = X_X^X + V_M^X + H_X$

where H is the enthalpy of vaporization. Equilibrium constants, K_M and K_X, can then be written for these two reactions, utilizing the appropriate metal and anion fugacities. A final condition defining crystal structures is that the number of sites, occupied or not, must be in the stoichiometric ratio. For a simple divalent binary compound, formula MX, this condition would be given by:

(24) $(M_M^X) + (V_M^X) + (V_M^{'}) + (V_M^{''}) = (X_X^X) + (V_X^X) + (V_X^{\cdot}) + (V_X^{\cdot\cdot})$. From this, the stoichiometric excess is:

(25) $\delta = (M_M^X) - (X_X^X) = (V_X^X) + (V_X^{\cdot}) - (V_M^X) - (V_M^{'}) + (V_X^{\cdot\cdot}) - (V_M^{''})$.

The case of a simple, univalent binary compound give eight unknowns ($V_M^{'}$, V_M^X, $V_X^{\cdot}$, V_X^X, e, h, P_M, P_X,) and six constants to relate them. For orthopyroxenes, the situation is complicated by the doubling of the positive charge (for Fe or Mg) and of the negative charge (for oxygen). The vacancies can then be doubly charged(relative to the normal charge state of the site), singly charged, or uncharged. For the doubly charged case, the equations above would not cover completely and we also need,

(26) $V_M^{'} = V_M^{''} + h^{\cdot} + E_{a2}$; $K_{a2} = \dfrac{(V_M^{''})(h^{\cdot})}{(V_M^X)}$

$$(27)\quad V_X^{\bullet} = V_X^{\bullet\bullet} + e' + E_{b2};\ K_{b2} = \frac{(V_X^{\bullet\bullet})(e')}{(V_X^{x})}$$

$$(28)\quad 0 = V_M'' + V_X^{\bullet\bullet} + E_{S''};\ K_S'' = (V_M'')(V_X^{\bullet\bullet})$$

Pyroxene would differ energetically from the simple binary approximation through bonding and entropy (three oxygens per divalent cation resulting in a higher entropy of formation for oxygen vacancies, oxygens differ in bond strength, etc.) but the stoichiometry of vacancy formation remains the same unless Si must be considered. However, silicon diffuses very slowly in most minerals, so it is likely that Si vacancies are unimportant. This approximation allows extension of simple defect balance theories to complex substances, such as minerals.

The solution of these equations is an imposing problem in the absence of knowledge about the various equilibrium constants, which have been worked out for but a few relatively simple substances. In addition, one must take into account impurities, which affect the other defects by acting as electron donors or acceptors. Fortunately, several approximations are available which allow some prediction of the behavior of a given system.

The first approximation to be made here is that impurities do not enter too strongly into the charge balance. This is a better approximation at higher temperatures where the intrinsic number of thermally induced defects is higher and those created by impurities is relatively less. A cation vacancy would likely be created by the presence of a

4+ ion, but this is much less common than other impurity types. Some of the impurities of different charge state (such as Na^{+} and Al^{3+}) are probably associated in pairs, rather than with defect sites; others will be associated with interstitial or vacancy creation in cation or anion sites, and alter the exact picture of crystal equilibrium. These may be neglected in determination of mechanism of diffusion.

The equations determining equilibrium in the crystal, therefore, are those designated above (Equations 17-28). An exact solution to them is not possible, but good approximations are possible if the various possibilities for maintaining electrical neutrality are treated separately, and the equations assumed independent. One must also designate relative values of equilibrium constants.

Nine ranges of defect balance are possible in a divalent binary crystal, and no modification is necessary for pyroxene equilibria. The ranges are, following Kroger (1964),

range I	$(h^{\cdot}) = (V_M^{'})$	range V	$(V_M^{'}) = (V_X^{\cdot})$
range II	$(h^{\cdot}) = 2(V_M^{''})$	range VI	$(V_M^{''}) = (V_X^{\cdot\cdot})$
range III	$(V_M^{'}) = 2(V_X^{\cdot\cdot})$	range VII	$2(V_M^{''}) = (V_X^{\cdot})$
range IV	$(e^{'}) = (h^{\cdot})$	range VIII	$(e^{'}) = 2(V_X^{\cdot\cdot})$
		range IX	$(e^{'}) = (V_X^{\cdot\cdot})$

Common cases for the relative sizes of the equilibrium constants are $K_S^{''} > K_i^2 > K_S^{'}$, and $K_S^{''} > K_S > K_i$. For each of these cases, we can solve the system of equations for any variable in terms of any other single variable. The most obvious choice for the independent variable is the

partial pressure of the anion, since it can be controlled by the use of various buffering mixtures. In the present study, the oxygen fugacity is controlled during the heating.

The results can be expressed in tabular form for either the ideal binary divalent crystal or for (divalent) orthopyroxenes. Since oxygen occurs as O_2 molecules, the relevant variable is $R = \frac{K_M K_{MO}}{fO_2^{\frac{1}{2}}}$ where

(29) $K_{MO} = f_M f_{O2} = K_S / K_M K_X$

Table 6 shows the functional relations between defect concentrations and R for different neutrality conditions, based of the work of Kroger (1964, pages 566-567). The charged defects are relevant to conductivity, while either charged or neutral vacancies may affect diffusion. In particular, if cation diffusion occurs by movement of cation vacancies, then the numbers of V_M^x, $V_M^{'}$, and $V_M^{''}$ are the factors controlling diffusion rate as partial pressure of oxygen is changed. If the diffusion occurred by interstitial movement, the number of interstitial cations would <u>decrease</u> with increasing anion partial pressure, while for vacancy types, the number of vacancies would <u>increase</u> in almost all cases. Thus at a given temperature, the diffusion rate would either increase or decrease with increasing fO_2, indicating the type of defect responsible for the diffusion. In the case of orthopyroxenes, the data show the defect type to be cation vacancies, by analogy with olivine (Buseck and Buening, 1973) and with most ionic compounds. The quality of the data is inadequate to show the functional dependence of rate on the oxygen fugacity so the charge of the predominant vacancy cannot be determined.

Table 6

Expressions for the concentrations of imperfections in a divalent binary compound (Kroger, 1964)

Range	e	h	(V'_M)	$(V^{\cdot}_X)$	(V''_M)	$(V^{\cdot\cdot}_X)$
I	$\left(\frac{K_i K_b}{K_{S'}}\right)^{\frac{1}{2}} R^{\frac{1}{2}}$	$\frac{K_S K_i}{K_b}^{\frac{1}{2}} R^{-\frac{1}{2}}$	$(K_a K_{S'})^{\frac{1}{2}} R^{-\frac{1}{2}}$	$\left(\frac{K_{S'} K_b}{K_i}\right)^{\frac{1}{2}} R^{\frac{1}{2}}$	K_{a2}	$\frac{K_{S'} K_{b2}}{K_i}$
II	$\left(\frac{K_i^2 K_b}{2K_{S'} K_{a2}}\right)^{\frac{1}{3}} R^{\frac{1}{3}}$	$\left(\frac{2K_i K_{S'} K_{a2}}{K_b}\right)^{\frac{1}{3}} R^{-\frac{1}{3}}$	$\left(\frac{K_i^2 K_{S'}^2}{2K_b^2 Ka2}\right)^{\frac{1}{3}} R^{-\frac{1}{3}}$	$\left(\frac{2K_{S'} K_b^2 K_{a2}}{K_i^2}\right)^{\frac{1}{3}} R^{\frac{2}{3}}$	$\left(\frac{K_i K_{S'} K_{a2}}{4K_b}\right)^{\frac{1}{3}} R^{-\frac{1}{3}}$	$\frac{K_{b2}}{K_i}\left(\frac{4K_{S'}^2 K_b K_{a2}}{K_i}\right)^{\frac{1}{3}} R^{\frac{1}{3}}$
III	$\left(\frac{2K_b^2 K_{b2}}{K_{S'}}\right)^{\frac{1}{3}} R^{\frac{2}{3}}$	$K_i\left(\frac{K_{S'}}{2K_b^2 K_{b2}}\right) R^{-\frac{2}{3}}$	$\left(\frac{2K_{S'}^2 K_{b2}}{K_b}\right)^{\frac{1}{3}} R^{-\frac{1}{3}}$	$\left(\frac{K_{S'} K_b}{2K_{b2}}\right)^{\frac{1}{3}} R^{\frac{1}{3}}$	$(2K_{S'}^2 K_b K_{b2})^{\frac{1}{3}} \frac{K_{a2}}{K_i} R^{\frac{1}{3}}$	$\left(\frac{K_{S'}^2 K_{b2}}{4K_b}\right)^{\frac{1}{3}} R^{-\frac{1}{3}}$
IV	$K_i^{\frac{1}{2}}$	$K_i^{\frac{1}{2}}$	$\frac{K_{S'} K_i^{\frac{1}{2}}}{K_b} R^{-1}$	$\frac{K_b}{K_i^{\frac{1}{2}}} R$	$\frac{K_{a2} K_{S'}}{K_b} R^{-1}$	$\frac{K_b K_{b2}}{K_i} R$
V	$\frac{K_b}{(K_{S'})^{\frac{1}{2}}} R$	$\frac{K_i (K_{S'})^{\frac{1}{2}}}{K_b} R^{-1}$	$(K_{S'})^{\frac{1}{2}}$	$(K_{S'})^{\frac{1}{2}}$	$\frac{K_{a2} K_b}{K_i} R$	$\frac{K_{b2} K_{S'}}{K_b} R^{-1}$
VI	$\left(\frac{K_b^2 K_{b2} K_i}{K_{a2} K_{S'}}\right)^{\frac{1}{4}} R^{\frac{1}{2}}$	$\left(\frac{K_i^3 K_{a2} K_{S'}}{K_b^2 K_{b2}}\right)^{\frac{1}{4}} R^{-\frac{1}{2}}$	$\left(\frac{K_{S'}^3 K_{b2} K_i}{K_b^2 K_{a2}}\right)^{\frac{1}{4}} R^{-\frac{1}{2}}$	$\left(\frac{K_{S'} K_{a2} K_b^2}{K_i K_{b2}}\right)^{\frac{1}{4}} R^{-\frac{1}{2}}$	$(K_{S''})^{\frac{1}{2}}$	$(K_{S''})^{\frac{1}{2}}$
VII	$\left(\frac{K_i K_b^2}{2K_{S'} K_{a2}}\right)^{\frac{1}{3}} R^{\frac{2}{3}}$	$\left(\frac{2K_i^2 K_{S'} K_{a2}}{K_b^2}\right)^{\frac{1}{3}} R^{-\frac{2}{3}}$	$\left(\frac{K_{S'}^2 K_i}{2K_b K_{a2}}\right)^{\frac{1}{3}} R^{-\frac{1}{3}}$	$\left(\frac{2K_{S'} K_b K_{a2}}{K_i}\right)^{\frac{1}{3}} R^{\frac{1}{3}}$	$\frac{1}{2}(V^{\cdot}_X)$	$K_{a2}\left(\frac{2K_{S'} K_{a2}}{K_i K_b^{\frac{1}{2}}}\right)^{\frac{2}{3}} R^{-\frac{2}{3}}$

Table 6 (continued)

VIII	$(2K_bK_{b2})^{\frac{1}{3}}R^{\frac{1}{3}}$	$\frac{K_i}{(2K_bK_{b2})}R^{-\frac{1}{3}}$	$K_S,(\frac{2K_{b2}}{K_b^2})^{\frac{1}{3}}R^{-\frac{2}{3}}$	$(\frac{K_b^2}{2K_{b2}})^{\frac{1}{3}}R^{\frac{2}{3}}$	$\frac{K_S,K_{a2}}{K_i}(\frac{4K_{b2}}{K_b})^{\frac{1}{3}}R^{-\frac{1}{3}}$	$(\frac{K_bK_{b2}}{4})^{\frac{1}{3}}R^{\frac{1}{3}}$
IX	$K_b^{\frac{1}{2}}R^{\frac{1}{2}}$	$\frac{K_i}{K_b^{\frac{1}{2}}}R^{-\frac{1}{2}}$	$\frac{K_S,}{K_b^{\frac{1}{2}}}R^{-\frac{1}{2}}$	$K_b^{\frac{1}{2}}R^{\frac{1}{2}}$	$\frac{K_S,K_{a2}}{K_i}$	K_{b2}

For all ranges, $(V_M{}^x)=\frac{K_iK_S,}{K_aK_b}R^{-1}$ and $(V_X{}^x)=R$

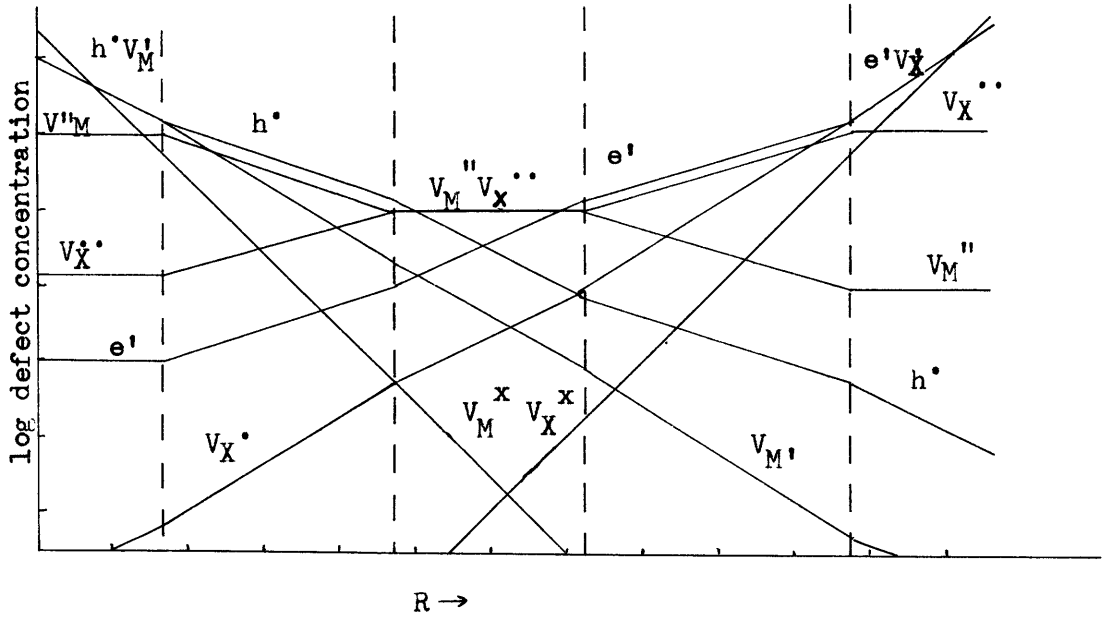
Data in which vacancy concentration is not buffered (Virgo and Hafner, 1969; Khristoforov et al., 1974) are not useful in analyzing kinetic behavior, as individual furnace runs may differ in vacancy concentration. Conditions in those studies were far too oxidizing to simulate natural magmas.

Other important data on transport properties of orthopyroxenes are contained in the work of Duba et al. (1973), and Boland et al.(1974). They have correlated changes in conductivity with direction, temperature, and oxygen fugacity for high quality natural single crystals. These data may be rationalized with the above model and results. Specifically, the conductivity increases with increase in temperature - a natural consequence of the increase in number of charged defects with temperature. This would be predicted whatever the nature of the charged defect, as the ionization of an uncharged defect is normally accompanied by an increase in entropy. The conductivity is highest in the c crystallographic direction, lowest in the b direction, intermediate in the a direction. This is not unreasonable, since bands of cations run parallel to the c axis in pyroxenes. No direct single crystal diffusion data are available to test the electronic or ionic nature of the responsible defects. It would seem likely that if ionic diffusion is found to be in agreement with these trends, it may indicate that this is the electrical conduction mechanism.

The dependence of conductivity on oxygen fugacity is somewhat complex. A minimum in conductivity is found by Duba et al. (1973) at about log fO_2 =

-10 at 1200°C. A possible interpretation of this phenomenon is a change in the nature of the carrier with increasing oxygen fugacity, perhaps from e' to $h^{\cdot}$ or from $V_X^{''}$ to $V_M^{\cdot\cdot}$ as shown in Figure 13 a and b, which are graphical solutions to the defect equations 17-28. Due to the relatively low energy required for formation of electron holes (which may be expressed as formation of Fe^{3+} from Fe^{2+}), and the evidence that vacancies are ionized in this way in olivine (Buseck and Buening, 1973), it may be that $K_{S''} > K_i^2 > K_{S'}$ or $K_{S''} > K_{S'} > K_i$, as assumed in Fig. 13a and b. The minimum in conductivity is probably due to a change from positive to negative in the major charge carrying defect. Since in this study disordering experiments were carried out under conditions more reducing than those used in the conductivity measurements, it would be expected that as the disordering rate for HCo increases with increasing oxygen fugacity, the conductivity would decrease. Except to say that the stoichiometric point is probably close in composition to the minimum in conductivity, the data do not allow the nature of the conduction mechanism to be determined. It is, however, fairly definite that cations move by vacancy diffusion. Whether most vacancies are charged as in olivine remains unknown.

At a given temperature, some vacancies are associated with impurities. At high temperatures, these are probably less important than the intrinsic population induced by thermal equilibrium. At the temperatures of the experiments performed in this study, they may be of some importance, but their effect cannot be ascertained from the present data. In any case, they would not change the basic conclusion about diffusion mechanism.



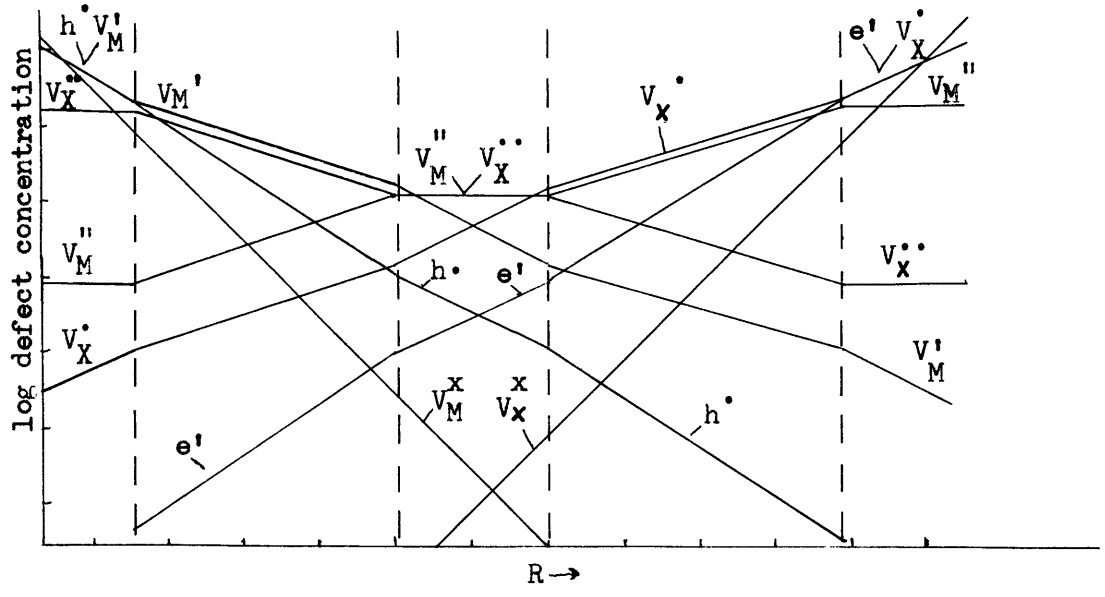


Figure 13

Variation of native imperfections with $R = \frac{K_M K_{MX}}{f_{X_2}^{\frac{1}{2}}}$.

Upper diagram, $K_S'' > K_i^2 > K_S'$

Lower diagram, $K_S'' > K_S' > K_i$

Many possible difficulties exist with this simplified model, but they will not be considered until more complete data are obtained, such as Hall coefficient measurements, further conductivity data, single crystal diffusion and radioactive tracer diffusion measurements.

The number of defects increases with temperature. The question then arises, does a pyroxene which disorders isothermally have a constant, equilibrium number of vacancies? This question is an important one if a more complete explanation of the experimental data is to be made. Thermally induced vacancies arise very rapidly. Their sources and sinks are not necessarily at crystal surfaces, but often are at screw dislocations and other extended defects (Shewmon, 1963). They are found to move rapidly through the crystal at relatively low temperatures, because the entropy term for such small concentrations makes their movement into the crystal energetically favorable.

Vacancies due to nonstoichiometry induced by the buffering gas mixture will be slightly slower when equilibrium is approached. The sources must be crystal surfaces exposed to the buffering mixture. Nevertheless, there is good evidence that equilibrium is approached fairly rapidly here, too, since the disordering rate is affected by the buffering mixture in times short relative to the disordering. Slight disequilibrium may remain, but it cannot easily be demonstrated. This same observation indicates that equilibrium is probable in the gas mixtures, too, a question that is not yet settled.

If diffusion of atoms occurs by vacancy exchange, then the diffusion

constants for the two species must be related. The form of the relation is:

(30) $D_M = fC_V D_V$

where D_M is the diffusion coefficient for the cation, f is a correlation factor, C_V is the concentration of the vacancies, and D_V is the diffusion coefficient for vacancies.

Chapter 7 ISOTHERMAL DISORDERING WITH TIME

If the number of vacancies in an isothermal disordering experiment is constant, then the rate is expected to be proportional to the difference in Gibbs free energy from the equilibrium state. If this free energy difference is known for all states through which the system passes while ordering or disordering, then integration should give the form of the disordering curve with time.

The first pyroxene disordering curve was that of Mueller (1969). He used the concentrations of iron in each site to define a rate equation based on traditional kinetic models:

$$(31) \quad \frac{-dX_{FeM1}}{dt} = -K_{12}X_{FeM1}(1-X_{FeM2}) + K_{21}X_{FeM2}(1-X_{FeM1})$$

where the K's are rate constants, the X's mole fraction site occupancies of iron, and t is time. Substitution $X_{FeM1} = 2x_{Fe} - X_{FeM2}$ where x_{Fe} is (Fe/Fe + Mg) for the crystal, and utilizing the distribution coefficient to relate the rate constants,

$$(32) \quad K_D = \frac{K_{21}}{K_{12}} = \frac{X^o_{FeM1}(1-X^o_{FeM2})}{X^o_{FeM2}(1-X^o_{FeM1})}$$

The rate equation can be integrated directly, and the form of the time - disorder curve worked out.

When the integrated form of this equation is applied to the data obtained in this study, it fits poorly. The rate falls off much faster

than is predicted by the equation. Picking any individual point as the starting point and using the known equilibrium value as the final point, the rate constant is always too high to predict the position of the next point correctly. The falloff in disordering rate with time is much greater than predicted by equation 31.

In an attempt to find a better relationship, the thermodynamic model of Saxena (1973) was applied to the data, so that a true equilibrium coefficient and actual values of activity could be determined, since it was shown by Saxena and Ghose (1971) that the assumption of ideality (used in the rate models of Virgo and Hafner(1969), and Mueller (1969)) is incorrect. In order to do this most directly, it is necessary to analyze the traditional rate equation, knowing that chemical potential differences are the driving forces for disordering.

The following discussion is based on that of Prigogine (1967), who discusses chemical kinetics and rate theory in the light of discoveries from the theory of irreversible thermodynamics, but modified to include the activity coefficients derived by the Saxena (1973) model. The basic postulates of irreversible thermodynamics are that systems evolve along a path of greatest probability (highest entropy)(this can be shown equivalent to maintaining lowest macroscopic Gibbs free energy), and that the rates of such processes are directly proportional to the difference in Gibbs free energy which drives the reaction.

A reaction coordinate is introduced to describe the extent of reaction. It is defined by: $\frac{dX_B}{\nu_B} = d\xi$ where dX_B is the change of mole

fraction of component B during time dt, and ν_B is the stoichiometric coefficient of B in the reaction, positive for the component increasing in mass. As an example, for the reaction $H_2 + I_2 = 2HI$, the extent of reaction $d\xi = \frac{dX_{HI}}{2} = -dX_{H_2} = -dX_{I_2}$.

One must then define the difference in free energy. An individual diffusing particle responds to its own gradient in chemical potential, but the system as a whole responds to the changes of the ensemble: as a particle moves, it displaces other particles, whose energies change. Prigogine uses the affinity function:

(33) $A = -\sum_i \nu_i \mu_i$

where ν_i is the stoichiometric coefficient of component i, and μ_i its chemical potential. At equilibrium, A = 0. It can be shown that $dS = \frac{Ad\xi}{T}$ for closed systems.

The velocity of a reaction is defined as:

(34) $v = \frac{d\xi}{dt}$.

Then the postulate of a chemical potential driving force gives

(35) $v = L(\frac{A}{T})$

where it is assumed that a linear relation exists, if deviation from equilibrium is not severe. Division by T shows that the probability of a system having a configuration with Gibbs free energy equal to G in some random walk process depends on a factor exp (-G/kT), and this "combines with the multiplicity of available configurations to give the compromise that maintains the system close to its most probable state of minimum macroscopic Gibbs function." (Flynn, 1972, p. 380).

The validity of the linear rate law must be proved in each case where it may be applied. In the present system, it is useful and instructive to show the relation between the linear law and the traditional kinetic laws for a chemical reaction.

The exchange reaction for disordering may be written:

(36) $Fe(M2) + Mg(M1) = Fe(M1) + Mg(M2)$

as before. The function A is then:

(37) $A = \mu_{FeM2} + \mu_{MgM1} - \mu_{FeM1} - \mu_{MgM2}$

The chemical potentials are calculated using the thermodynamic model of the last section. They are:

(38)
$$\mu_{FeM1} = \mu^{\circ}_{FeM1} + RT \ln (X_{FeM1}) + RT \ln \gamma_{FeM1}$$
$$\mu_{FeM2} = \mu^{\circ}_{FeM2} + RT \ln (X_{FeM2}) + RT \ln \gamma_{FeM2}$$
$$\mu_{MgM1} = \mu^{\circ}_{MgM1} + RT \ln (1-X_{FeM1}) + RT \ln \gamma_{MgM1}$$
$$\mu_{MgM2} = \mu^{\circ}_{MgM2} + RT \ln (1-X_{FeM2}) + RT \ln \gamma_{MgM2}$$

Where μ is the chemical potential of a pure end member, X is the mole fractions of the cation in the site, and γ is the activity coefficient. The μ° values are obtained from the equilibrium value of the mole fractions, so that their differences in equation 37 give rise to a log K term, where K is the <u>equilibrium</u> constant and contains equilibrium values of the activity. The activity coefficients are obtained from the least squares fit of equilibrium data from various compositions, as outlined in the previous section. Then,

(39) $RT \ln \gamma_{FeM1} = \frac{W_{M1}}{RT} (1-X_{FeM1})^2$

with W the value of the energy constant for the appropriate site. Substituting these values for the activity coefficients in equation 37, and combining terms,

$$(40)\quad A = -RT \ln \frac{(1-X_{FeM1})(2X_{Fe} - X_{FeM1})(X^{o}_{FeM1})(1-2X_{Fe} + X^{o}_{FeM1})}{(X_{FeM1})(1-2X_{Fe} + X_{FeM1})(2X_{Fe} - X^{o}_{FeM1})(1 - X^{o}_{FeM1})}$$
$$+ W_{M1}((1-X^{o}_{FeM1})^2 - (X^{o}_{FeM1})^2 + (X_{FeM1})^2 - (1-X_{FeM1})^2)$$
$$+ W_{M2}((2X_{Fe} - X^{o}_{FeM1})^2 - (1 - 2X_{Fe} + X^{o}_{FeM1})^2 + (1-2X_{Fe} + X_{FeM1})^2$$
$$- (2X_{Fe} - X_{FeM1})^2)$$

where X_{Fe} is the mole fraction Fe/Fe + Mg for the mineral, T is the temperature of disordering, X_{FeM1} is the instantaneous value of mole fraction of iron in site M1 and X_{FeM1} is the mole fraction of iron in M1 at equilibrium for temperature T.

The usual formulation of reaction rate is given by:

$$(41)\quad v = v_{12} - v_{21} = k_{12} X_{FeM2} X_{MgM1} - k_{21} X_{FeM1} X_{MgM2}$$
$$= k_{12} X_{FeM2}(1-X_{FeM1}) - k_{21} X_{FeM1}(1-X_{FeM2})$$

This formulation was developed for reactions in gases. For solutions, the activity coefficients are usually added to the concentration terms. In addition, the two terms on the right hand side of the equation are often multiplied by a factor β which may be dependent on composition (Denbigh, 1966). Then,

$$(42)\quad v = k_{12} X_{FeM2} \gamma_{FeM2} (1-X_{FeM1}) \gamma_{MgM1} \beta - k_{21} X_{FeM1} \gamma_{FeM1} (1-X_{FeM2}) \gamma_{MgM2} \beta$$

Expanding,

$$(43)\quad v = k_{12}X_{FeM2}\gamma_{FeM2}(1-X_{FeM1})\gamma_{MgM1}\beta\left(1-\frac{k21X_{FeM1}\gamma_{FeM1}(1-X_{FeM2})\gamma_{MgM2}\beta}{k_{12}\,X_{FeM2}\gamma_{FeM2}(1-X_{FeM1})\gamma_{MgM1}\beta}\right)$$

It is well known that K, the equilibrium constant, $= k_{12}/k_{21}$. Then,

$$(44)\quad K = \frac{(X^{\circ}_{FeM1})(\gamma^{\circ}_{FeM1})(1-X^{\circ}_{FeM2})(\gamma^{\circ}_{MgM2})}{(X^{\circ}_{FeM2})(\gamma^{\circ}_{FeM2})(1-X^{\circ}_{FeM1})(\gamma^{\circ}_{MgM1})} = \frac{k_{12}}{k_{21}}$$

Substituting the value of k_{12}/k_{21} back in equation 43, the value of the term subtracted from one becomes identical to the log part of equation 40 (the β terms cancel here). Then,

$$(45)\quad v = k_{12}X_{FeM2}\gamma_{FeM2}(1-X_{FeM1})\gamma_{MgM1}\left(1 - \exp\left(-\frac{A}{RT}\right)\right)$$

This equation is then in the form predicted for a diffusion flux equation(16). There is a term expressing a difference in chemical potential, a term expressing the concentration of species experiencing this driving force, and various terms which express the mobility of the species. The value of k_{12} is determined by experiment, the activity coefficients determined by equation 39, and β is initially assumed constant and simply incorporated into k_{12}. This equation must then be integrated in order to obtain change in mole fraction of any site with time. Since the equation may be set up with X_{FeM1} as the only variable (by the substitution $X_{FeM2} = 2X_{Fe} - X_{Fem1}$), that may be substituted for $d\xi$, and the velocity becomes dX_{FeM1}/dt.

Integration of this equation is not easily accomplished with an analytic function. The most direct approach is to use a numerical integration routine, which is not tedious when programmed into a computer. The routine chosen here was the Runge-Kutta method (Ross, 1964).

This calculates accurate approximations to the initial value problem, $dy/dx = f(x,y)$, $y(x_o) = y_o$ without using especially small intervals along x.

The problem in each step is to find y(1) for x(1) = x(0) + h. This is then used to find y(2) from x(1) + h, and so on. The following constants are calculated for each step:

(46) $k_1 = hf(x_o,y_o)$

(47) $k_2 = hf(x_o + h/2,\ y_o + k_1/2)$

(48) $k_3 = hf(x_o + h/2,\ y_o + k_2/2)$

(49) $k_4 = hf(x_o + h,\ y_o + k3)$

(50) $K_o = \frac{1}{6}(k_1 + 2k_2 + 2k_3 + k_4)$

Then set $y_1 = y_o + K_o$, and proceed to the next step. It is possible to use a simpler method after the first four steps have the integration well started, but this was not done.

Since there is an adjustable constant in the equation to be integrated ($k_{12}\beta$), both sides of equation 45 were divided by $k_{12}\beta$, assuming β to be independent of composition. Thus the time scale became arbitrary (although linear), and disordering data should fit the calculated curve by simply scaling the time by a constant factor. With the equation and integrating routine set up on the computer, it became a simple matter to vary the parameters X_{Fe}, X^{o}_{FeM1}, X^{i}_{FeM1}, W_{M1}, W_{M2}, and T, where X^{i}_{FeM1} is the initial, ordered value of the parameter. Figures 14 and 15 show the form of the curves at 700°C and 800°C predicted by this equation.

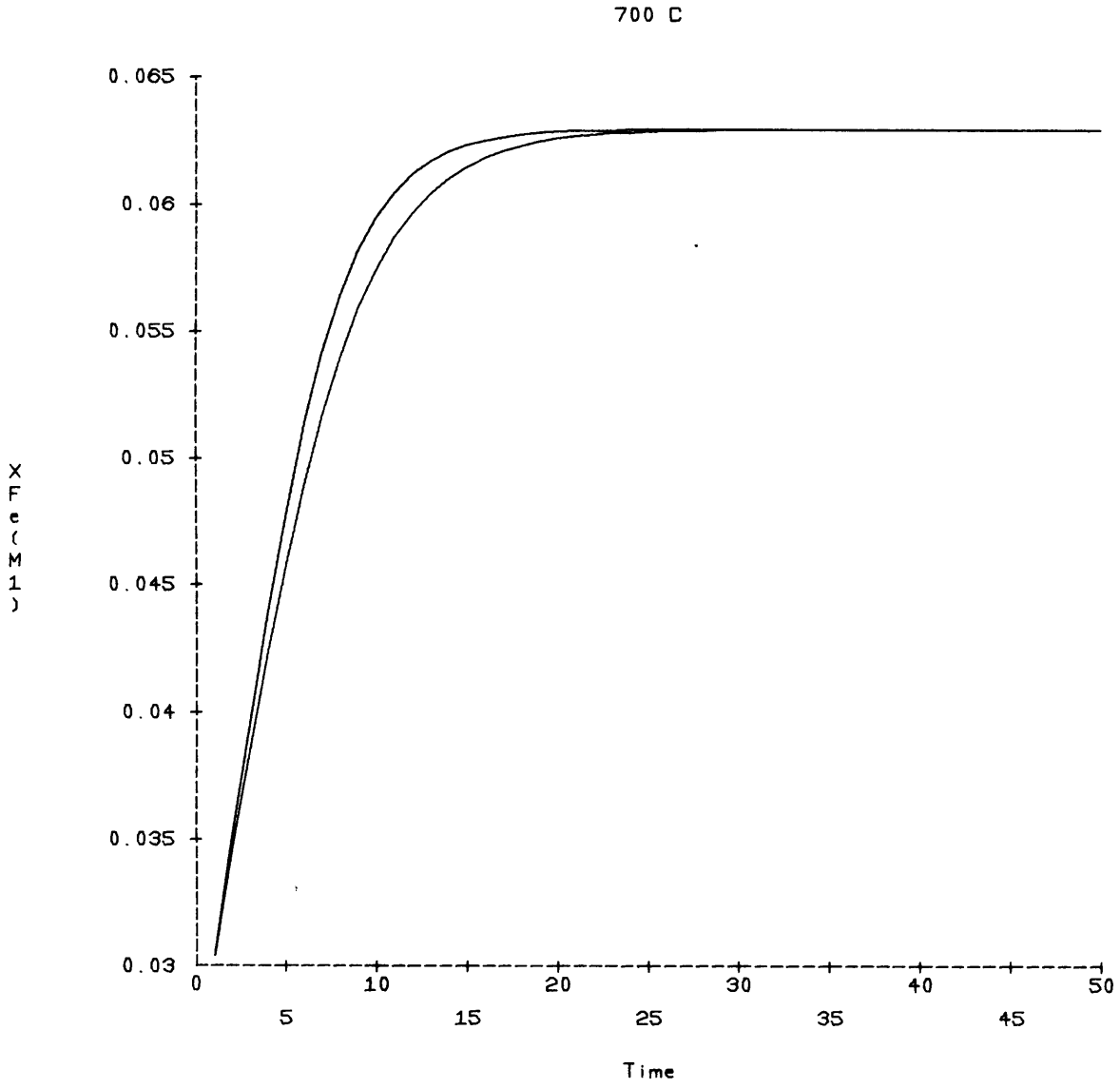


Figure 14 Mole fraction Fe^{2+} in M1 site with time (700°C) (arbitrary time scale). Upper curve, W's = 0. Lower curve, W_{M1} = 2334 cal/mole, W_{M2} = 1974 cal/mole.
Model calculation.

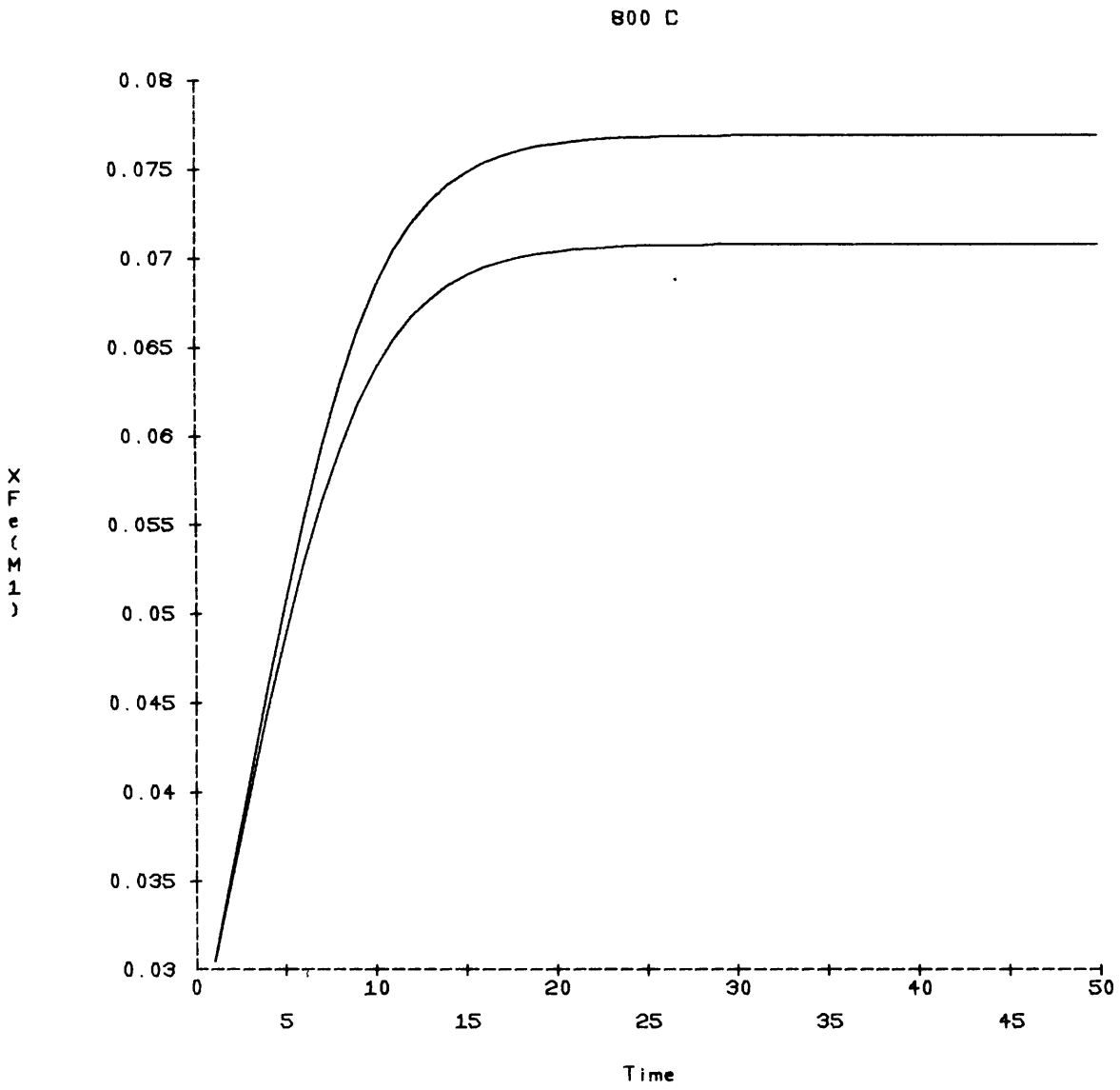


Figure 15 Mole fraction Fe^{2+} in M1 site with time (800°C) (arbitrary time scale). Upper curve to fit maximum value of disorder, lower curve to fit final value of disorder.
Model calculation.

Figure 14 shows two curves at 700°C, the upper representing the form of the equation if the energy parameter W is set to zero for each site, the lower curve representing the form if the W's are set to the values derived in chapter 5, W_{M1} = 2334.05, and W_{M2} = 1974.15. The time scale is arbitrary, and should be linear if β is independent of composition and degree of disorder. However, just as is the case in the Mueller equation (31), the rate of disordering falls off more sharply than the model predicts. Figure 15 shows two curves at 800°C with different values for final equilibrium; one corresponds to the longest time of disordering, the other to the maximum degree of disorder, reached in just over an hour. Even for samples run for the very shortest times, 5, 12, and 20 minutes, a falloff from these curves was discernable. No data are plotted, because a constant value of $k_{12}\beta$ (necessary to specify a time scale) is not obtained.

There are at least three possible reasons why this falloff in rate might occur. The first is that cation vacancy concentration decreases during the experiment. This is possible but perhaps less likely due to reasons set forth in the discussion of vacancy equilibrium. A second possibility is the hypothesis of Gray (1974), who predicted just such a falloff in rate because of the constrained nature of the interchange - in the case of ordering, the exchange within M1M2 chains occurring more readily than exchange between chains. Very local exchanges would begin the ordering, but longer range exchanges would become necessary as parts of the chain became almost totally ordered.

If, for instance, the M1 and M2 sites are considered as pairs, and no exchange is possible between pairs, then a pair which starts with two Fe atoms would not be able to order. This assumption is perhaps less justified in the case of disordering, where any ordered region of the crystal can be totally disordered, in theory, by the single passage down the chain of a cation vacancy, but may hold.

A better test of Gray's hypothesis is made if the pyroxene has a ration Fe/ Fe + Mg close to .50. The reason can be visualized using figure 16, a diagrammatic sketch of the octahedral chains in ortho-pyroxene. The M1 sites form a "street" with M2 sites as side avenues. Assume that initially no exchange occurs except within the chains. As ordering occurs, there would be a great number of exchanges which would occur very quickly, as they involve only one or two exchanges to produce the ordering. As the reaction progresses, however, more and more exchanges are needed to move an atom of iron down a chain until a vacant M2 site is available (a "musical chairs" effect).

If the total iron in the sample is much lower, fewer exchanges would be needed to move an iron atom adjacent to a magnesium-filled M2 site with which it could exchange, and the effect would not be as great. A similar situation would develop if the crystal was very iron rich, as then few exchanges would be needed to bring a magnesium atom adjacent to a M1 site filled with iron. Thus, one might expect that if Gray's hypothesis was true, low and high iron samples should disorder and order more quickly than intermediate ones; this seems to be the case when HCo

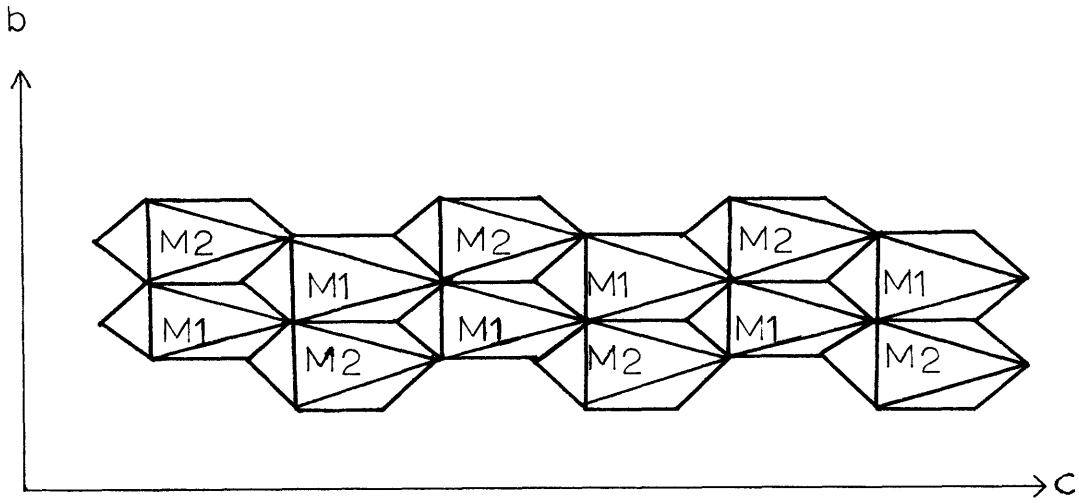


Figure 16 Sketch of pyroxene chain of octahedral sites

is contrasted with the data of Kristoforov et al. (1974).

A secondary effect would be observed if exchange between chains were necessary to further disorder or order the crystal, assuming exchange between chains occurred more slowly than within them (which would agree with the conductivity data of Duba et al., 1973). If a chain had a higher iron content than a neighbor (for any reason), disordering and ordering would be controlled by this lower rate for longer times.

Data on such a system are discussed by Khristoforov et al.(1974). They disordered an orthopyroxene, Fe/Fe + Mg = .57 in a vacuum at temperatures of 500, 700, and 900°C for periods of 1 to 240 hours. Their data do not show a maximum like HCo. They describe the disordering as a two-stage process, with one rapid, initial stage, and a slower second stage. Plotting their data on a ln (X_{FeM2}) vs. t plot, they fit two straight lines to the data and derive equations to fit the two lines. Unfortunately, they do not plot all the data given in the paper, and when all data are plotted the scatter from their model is much higher. Gray's hypothesis of geometric inhibition of disordering may hold here. Plotting the data for sample HCo at 700°C on such a semilog plot produces only a continuous curve, suggesting that no two-stage process is operative (see Fig. 12).

A third possible reason for a falloff of rate is that there is some competing rate process which simultaneously lowers the Fe population in M1 as disordering raises it. The 800°C data show that some such process must exist to explain the maximum in the data and subsequent falloff in

M1 iron with time. One hypothesis is that it is due to the sheared nature of the sample.

Boland et al.(1974) have shown that homogenization of clinopyroxene lamellae occurs at temperatures between 800°C and 1000°C, and possibly at lower temperatures. They found that electrical conductivity decreased with time at these temperatures, and verified by electron microscopy and optic examination that lamellae were indeed homogenized at these temperatures. They state that the lamellae were not produced by exsolution, but that shear-produced clinopyroxene lamellae may have been slightly enriched in Ca and Fe by later diffusion. Large numbers of lamellae similar to these appear in sample HCo, as verified both by electron microscopy and by optical examination.

The structure of lamellae similar to these has been investigated by Buseck and Iijima,(1974). They confirmed that microtwinning explains the polymorphism of orthorhombic and monoclinic enstatite. If such shear induced lamellae are present, they may be unstable and disappear with time by diffusion. Such twinning may occur on a unit cell scale.

This phenomenon can produce the observed results. About 2.5% of the iron in the sample must be affected, since that amount was apparently removed from the M2 site to the M1 site after the disorder reached a maximum. One hypothesis is that calcium in the clinopyroxene lamellae may be affecting the Mossbauer spectra, as discussed by Dowty and Lindsley (1973). With only .6% CaO present, of .02 Ca ions per 6 oxygens, it is highly unlikely that sufficient concentration exists to affect 2.5%

of the sites enough to explain the observed effect, even if the Fe were concentrated entirely in lamellae. It is quite possible, however, that the lamellae do affect the Mossbauer spectra.

A more likely mechanism is clustering of iron resulting in higher M1 occupancy. This may not have been found by microprobe analysis because the scale of the inhomogeneity was too small. If calcium is also concentrated in lamellae, the increase in M1 iron would be even greater. As the lamellae dissolve, the small amounts or iron and calcium there would redistribute throughout the crystal, causing a falloff in M1 occupancy with time, as observed. The 800°C data show this falloff clearly, and the 700°C data show it as a falloff in disordering rate. This effect might also be found about the tiny inclusions of iron chrome spinel, approximate formula $(Fe^{2+}_{1.91}Mg^{2+}_{.09})(Fe^{3+}_{1.21}Cr^{3+}_{.75}Al^{3+}_{.04})\ O_4$. These are too minor to greatly affect the system (no spectral contribution from iron in the chromite could be resolved in either heated or unheated samples), but they may add to the observed effect by producing local areas of the pyroxene more iron rich than the whole as they dissolve. None of these effects is proven, but no better explanation seems possible with the present data.

Discarded hypotheses which were also considered include: (1) distortion of sites near lamellae, either by calcium or by surface effects, (this would boost apparent M2 occupancy by lowering quadrupole splitting of the M1 sites, but it is apparently M1 occupancy that is high in unheated samples); (2) diffusion of iron into the lamellae (but the

lamellae disappear); (3) some contribution to the M1 Mossbauer peaks from the chromite(but they are not expected to fall near the position of the M1 orthopyroxene peaks, as the value of isomer shift is expected to be higher, Imbert and Martel (1965)); and (4) some domain structure (none has been observed in pyroxenes). The possible occurrence of this effect in a relatively pure orthopyroxene suggests that caution should be taken when working with sheared pyroxenes. The recent work of Boyd (1974) may be cited as one example in which sheared pyroxenes play a prominent role.

Chapter 8 APPLICATIONS OF ORDER-DISORDER IN ORTHOPYROXENES TO NATURAL PROCESSES

Second only to crystallization, ordering and disordering rates are probably the fastest chemical changes in pyroxenes. Most geologic phenomena occur on a much longer time scale, thus potential applications are limited. However, Fe-Mg ordering may help solve several classes of problems.

Shock metamorphism is one such area of application. High disorder in naturally shocked pyroxenes from lunar samples was found by Dundon and Hafner (1971). They assumed impact heating was the cause, and estimated a maximum temperature, using kinetic arguments. Due both to extensive assumptions and the undoubted shearing of the sample, their result is questionable. More work is needed on the effects of shock to arrive at a solution. Cation ordering may be an important tool in unravelling the thermal history of pyroxenes during and after shock, ordinary interphase equilibria being too slow to provide useful input.

Order-disorder data may help describe the cooling histories of volcanic rocks. Lavas can cool in seconds, or in months, slower cooling sometimes allowing alteration of equilibrium mineral assemblages. Highly disordered pyroxenes prove that rapid cooling has taken place and interphase equilibria quenched. Elemental distributions are probably better indicators of magmatic temperatures in rocks with significantly disordered pyroxenes than in those where ordered pyroxenes are found.

Models of element distribution in minerals may also depend on order-disorder. Grover (1974), Saxena (1973), and others discussed the relationship between activity coefficients describing intercrystalline exchange, and intracrystalline order-disorder. This effect, although probably small, must be investigated if an accurate predictive model of elemental distribution is desired, rather than simple empirical relationships such as the two-pyroxene geothermometer used by Boyd (1974).

Another possible application is in potassium argon dating of whole rock basalts. This dating method assumes that no contamination of the rock by excess Ar^{40} has taken place (i.e., complete outgassing has occurred). Rapidly cooled rocks almost certainly will incorporate any Ar^{40} contained in the melt, while more slowly cooled ones are likely to be outgassed. Pyroxene disorder may indicate that the sample should be discarded.

Studies of kimberlite emplacement, of potential economic importance in diamond mining, may be aided by order-disorder data. McGetchin and Ullrich (1973), presenting a theoretical analysis of kimberlite eruption mechanisms, predicted possible surface eruption velocities as high as 700 meters/second, with adiabatic expansion of gases cooling the fluidised material to -20°C. This result would help explain the presence of charred wood and unaltered coal deep within kimberlite pipes (Williams, 1932).

Since kimberlite was predicted to take approximately one hour to

ascend from the mantle (McGetchin and Ullrich, 1973), the magma probably remained isothermal until almost reaching the surface. Lowered pressure allowed CO_2 and H_2O to come out of solution, resulting in explosive expansion and adiabatic cooling. Such rapid quenching might allow use of Fe-Mg order as a geothermometer, to ascertain the original temperature of the magma and xenoliths. If the model is correct, large xenoliths, initially homogeneous in temperature, should have disordered exteriors quenched by the cold gases but more ordered interiors resulting from slower cooling.

As eruption subsides, a mixture of hot and cold material would fill the diatreme. Deeper parts of the diatreme, with fewer cooled xenoliths, probably remained at elevated temperatures. Disorder-depth relationships for xenoliths of similar composition may reveal some details of this final temperature distribution.

Exposure to high temperature, low pressure, and high fCO_2, resulting in pitting and graphitization of diamonds (Harris and Vance, 1974), may explain why diamonds are absent in well-indurated "hardebank" kimberlite while overlying, softer kimberlite gives high yields (Williams, 1932). Conceivably, order-disorder surveys of kimberlite deposits will provide information on the probability of diamond preservation, aiding both in exploration and in development. High disorder would be a good indication of the rapid quench needed for diamond preservation.

To ascertain the validity of the method, a websterite xenolith,

from the Moses Rock kimberlite dike in Utah, was obtained from Dr. T.R. McGetchin. A point count of the unaltered material in this sample showed it to contain 53% orthopyroxene and 47% clinopyroxene. The ratio Fe/Fe + Mg for this opx is .126 (as determined by partial microprobe analysis at Caltech by Dr. McGetchin), only slightly lower than for sample HCo (Fe/Fe + Mg = .131). Magnetic separation and hand-picking produced an almost pure orthopyroxene separate, which was then prepared in the same way as the Mossbauer samples of the HCo orthopyroxene.

The near complete overlap of the two low velocity Mossbauer peaks complicated fitting of the spectrum. This problem was overcome by fitting four peaks (two for possible ferric ion) to the low velocity region, constraining them to be constant, and fitting the two high velocity peaks without constraints. Convergence of the calculated spectrum to the data resulted; T(M1) was found to be .440.

Several explanations are possible for the very high disorder. Some clinoenstatite might have been produced during inversion from protoenstatite if the quenching occurred from above 1000°C (Smyth, 1971), and this may affect the spectrum. While CaO is low (0.37%), Al_2O_3 is quite high (7,24%) and may affect cation site occupancies. Although further study is necessary, it seems likely that rapid quenching has occurred, and the McGetchin - Ullrich model qualitatively justified.

In conclusion, much has been learned and much remains to be done. More data on other compositions are needed to test the disordering and

ordering model used, and to verify Gray's hypothesis of geometric restrictions on ordering rates. Reversibility of the proposed equilibrium distribution determined for HCo must be demonstrated by ordering experiments. More conductivity data, Hall effect measurements, and diffusion measurements are needed to verify proposed transport models. It should be possible to derive useful information from natural pyroxene disorder, but useful input into quantitative models of rapid processes such as kimberlite genesis awaits more experimental work.

APPENDIX A

A FORTRAN IV program was written to find the volume percent CO_2 (known as VOLPER) in a mixture of CO_2 and H_2 that produces at equilibrium a given value for oxygen fugacity (log fO_2 is LFO2 in the program) at a given absolute temperature and a total pressure of one atmosphere. The data section takes values of free energy of formation for CO_2, CO, and H_2O, one set for each end of a 100°K temperature range, (total of six values), the lower temperature of the two extremes, and an estimated initial value of log fO_2 to use as a limit for the calculations in that temperature range, on each card. The output consists of blocks of data, each representing one five degree Kelvin step, with values of LFO2 and VOLPER alternating. A sample set of data from Robie and Waldbaum (1968) are included, separated from the main body of the program by a $ENTRY line as would be used in WATFIV compilers. Also, no provision is made for running more than one data card at a time, although that could easily be added. This program is made obsolete by the work of Deines et al.(1974). The listing of the program deck follows.

```
      REAL K1,K21,LFO2
      DIMENSION VOLPE(4),AFO2(5)
  100 READ(5,11)T,GC01,GC021,GH201,GC02,GC022,GH202,LFO2
      WRITE(6,11)T,GC01,GC021,GH201,GC02,GC022,GH202,LFO2
   11 FORMAT(F5.0,6F7.0,F4.0)
      X=(GC02-GC01)/20
      Y=(GC022-GC021)/20
      Z=(GH202-GH201)/20
   10 FORMAT(1X,F5.0,7H TEMP K)
      DO 15 J=1,20
      WRITE(6,10)T
      K1=EXP(+(GC021-GC01)/(1.98717*T))
      K21=EXP(+(GH201)/(1.98717*T))
      AFO2(1)=LFO2
      DO 25 K=1,75
      DO 20 I=1,4
      E=+2.302585*AFO2(I)
      FO2=EXP(E)
      A=SQRT(FO2)
      VOLPE(I)=100*(1+(A/K1))/(2+(A/K1)+(K21/A))
      AFO2(I+1)=AFO2(I)+.05
   20 CONTINUE
      WRITE(6,12)(AFO2(I),VOLPE(I),I=1,4)
      AFO2(1)=AFO2(4)+.05
   25 CONTINUE
      T=T+5.
      GC01=GC01+X
      GC021=GC021+Y
      GH201=GH201+Z
   15 CONTINUE
   12 FORMAT(1X,4(6H LFO2 F6.2,8H VOLPER F8.4))
      STOP
      END
$ENTRY
 800.-43609.-94539.-48644.-45739.-94577.-47353.-32.
 900.-45739.-94577.-47353.-47854.-94609.-46040.-30.
1000.-47854.-94609.-46040.-49956.-94636.-44709.-27.
1100.-49956.-94636.-44709.-52044.-94657.-43373.-25.
1200.-52044.-94657.-43373.-54120.-94675.-42028.-23.
1300.-54120.-94675.-42028.-56183.-94688.-40663.-21.
1400.-56183.-94688.-40663.-58235.-94700.-39302.-20.
1500.-58235.-94700.-39302.-60277.-94710.-37929.-19.
```

APPENDIX B

As peak intensity is the most important parameter measured in the Mossbauer spectra obtained during this study, the purpose of this appendix is to examine the major effects responsible for observed intensities, with the exception of line shape theory. The most important effects are the fraction of recoilless emissions and absorptions, and the polarization of the gamma rays.

The origin of the measured parameters is important in any discussion of the intensities. The isomer shift measures the energy displacement from a standard of the midpoint of a spectrum arising from iron in one crystallographically distinct site. The gamma emission is accompanied by a change in nuclear volume (for Fe57 the nucleus expands on emission). One can model the nucleus as a homogeneous sphere with electrostatic energy related to the nuclear radius (Wertheim, 1964). The energy difference between a point and finite nucleus may be expressed by:

(51) $$\delta E = \int_0^\infty \rho (V - V_{pt})\, 4\pi r^2\, dr = -\frac{2\pi}{5} Ze^2 |\psi(0)|^2 R^2$$

where $-e|\psi(0)|^2 \equiv \rho$ = electronic charge density at the nucleus,

V_{pt} is the electrostatic potential for a point nucleus

V is the electrostatic potential for a finite nucleus

Z is the atomic number

e is a unit charge

r is the radius of the nucleus.

Then the energy difference between excited and ground states is $\delta E_{ex} - \delta E_{gd} = \frac{2\pi}{5} Ze^2 |\Psi(0)|^2 (R_{ex}^2 - R_{gd}^2)$. The <u>difference</u> in radius between ground and excited states, characteristic of a given nucleus and ρ the charge density, varying with environment, are thus the important factors. Various electrons contribute to $\Psi(0)$, especially s and d orbitals.

The energy levels for a spherically symmetric nucleus may be split into 2I+1 different energies if the sphericity or uniformity of nuclear charge density changes. The result of making the nucleus oblate or prolate is to change internal energy levels, giving it a quadrupole moment. This discussion follows that of Feynman , v. II, sections 6-5.

The electric potential produced by some arbitrary set of charges i is given precisely by:

(52) $V = \frac{1}{4\pi\epsilon_o} \sum_i \frac{q_i}{r_i}$

where ϵ_i is a constant, q_i is the charge on a particle of distance r_i from the point P where the field is measured (Fig. 17). Ordinarily, the observer is a great distance, R, from the set of charges, and the equation reduces to:

(53) $V = \frac{1}{4\pi\epsilon_o R} \sum q_i$

The sum acts as a point charge, However, if the positive and negative charges balance, then one needs to look closer. Charge separation means that a field exists, but $r_i \neq R$. Choose an observation point P, of distance R from an arbitrary point within the charges. Let $\vec{d}_i$ be the

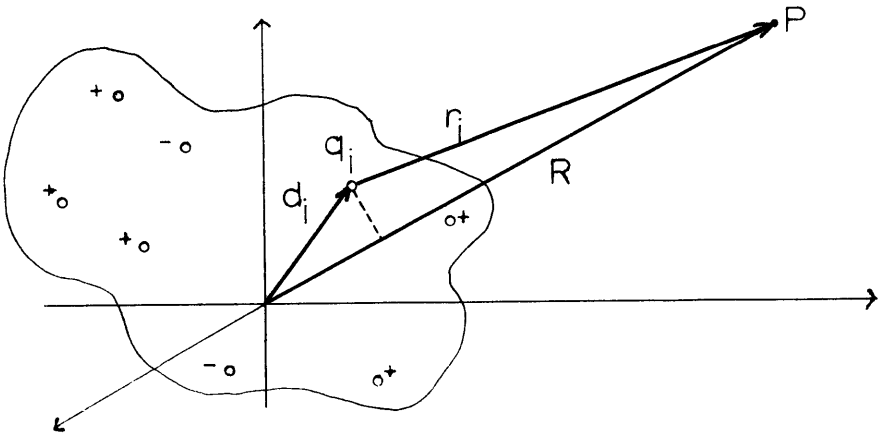


Figure 17 Determination of quadrupole moment

vector from the arbitrary point to charge q_i. The difference between r_i and R will be the projection of $\vec{d}_i$ on $\vec{R}$. If $\hat{e}_r$ is the unit vector in the direction of $\vec{R}$ (i.e. $\vec{R}$ is an arbitrary scalar times this unit vector) then, still seeking a value for $\vec{r}_i$ to put into the precise equation for ϕ:

(54) $\vec{r}_i \approx \vec{R} - \vec{d}_i \cdot \vec{e}_r$

(55) $\frac{1}{\vec{r}_i} \quad \frac{1}{\vec{R}} \left(1 + \frac{\vec{d}_i \cdot \vec{e}_r}{\vec{R}} + \frac{(\vec{d}_i \cdot \vec{e}_r)^2}{R^2} + \ldots \right)$ using the binomial theorem expansion. Then,

(56) $V = \frac{1}{4\pi\epsilon_o} \left(\frac{Q}{R} + \sum q_i \frac{\vec{d}_i \cdot \vec{e}_r}{R^2} + \ldots \right)$

If the system is neutral, the first term drops out (it is the potential for large R). The second term is the dipole potential

(57) $V_d = \frac{1}{4\pi\epsilon_o} \frac{(\sum q_i \vec{d}_i) \cdot \vec{e}_r}{R^2}$

This potential has an inverse R^2 dependence. Also, since there is a dot product, the angular dependence is cos θ, and the dipole potential will vanish when $\theta = 90^o$. It will also disappear (more importantly) if the molecular symmetry causes it to do so (such as in CO_2, a linear molecule). The quadrupole potential now becomes important. It is the analogous term of the series with inverse R^3 dependence.

(58) $V_Q = \frac{1}{4\pi\epsilon_o} \frac{(\sum q_i \vec{d}_i) \cdot \vec{e}_r)^2}{R^3}$

In the case of a nucleus, if the nuclear volume is approximately a spherical mass of protons with the electron density spherically distributed about it (as for a neutral atom), any 1/R term is eliminated.

Nuclei with spin $\frac{1}{2}$ have a magnetic dipole moment, but no electric dipole moment. If the nucleus is a prolate or oblate spheroid, it will have an electric quadrupole moment (this is the case of I = 3/2). This moment will interact with any electric field gradient to produce a splitting of the 2I + 1 degenerate, I = 3/2 state, into two levels $m_I = \pm 3/2$ and $m_I = \pm \frac{1}{2}$. Thus the transitions are from the I = 3/2, $m_I = \pm \frac{1}{2}$, and from the I = 3/2, $m_I = \pm 3/2$ states to the ground state $I = \frac{1}{2}, m_I = \pm \frac{1}{2}$. The twofold degeneracy may be removed by adding a magnetic field, which, with the selection rules, shows six different allowed transitions, between combinations of six separate energy levels, even if the electric field gradient is absent (as in cubic coordination).

The following discussion is based on that of Stöckler and Sano, 1970.

One factor to be treated when discussing orientation effects of spectra in single crystals is the "Mossbauer fraction", which expresses the fraction of gamma rays emitted that are recoilless. This is directly related to the Debye-Waller factor obtained from x-ray diffraction studies. If $\vec{k}$ is the wave vector of the gamma radiation (magnitude is the energy of the quantum, direction is that of the gamma propagation) and $\vec{u}_r$ is the ensemble average of the instantaneous displacement of nucleus r from its mean position, then the Mossbauer fraction fa is given by

$$(59) \quad f_a = |\langle i|\exp(i\vec{k} \cdot \vec{u}_r)|\, j\rangle|^2$$

where i and j are the initial and final lattice states, and this expression indicates a thermal average over the states. An approximation good

for the case of harmonic lattice vibrations is

(60) $f_a = \exp\left[-\langle(\vec{k} \cdot \vec{u}_r)^2\rangle\right]$

The net result is that f_a is smaller when the atom is less tightly bound. This occurs at higher temperatures, which is one reason to cool the system. More importantly, however, this factor can vary with direction in crystals, because atoms are often bound more tightly in one direction than in another. Thus a measurement of f_a with direction can help describe the potential field holding the atom in its place.

A treatment of $\langle u_r^2\rangle$ might divide the motions into two components- one which is a rigid body anisotropic mean square displacement tensor U, and the nonrigid body distortional vibration component $\langle u^2\rangle_d$, giving

(61) $\langle u_r^2\rangle = \sum_{ij} U^{ij} l_i l_j + \langle u_r^2\rangle_d$

for displacement of atom r in direction l. Note that tensors are a class of things including scalars (zeroth order tensor), vectors (first order tensors), and tensors of higher orders. $\langle U^{ij}\rangle$ is a second order tensor. It has two superscripts, and may be specified by a matrix. Since any direction l may be specified using a combination of three vectors (the basis vectors), and in particular as linear combinations of the three unit vectors along the Cartesian coordinate axes (or along the crystallographic axes), it is evident that i and j are either 1,2,or 3, so a 3x3 matrix describes U, and l_i and l_j are any two column vectors. The argument can be specified even for a triclinic case, using various assumptions, until a final value for $\langle u_r^2\rangle$ is found, referred to the the crystal axes. The usefulness of the tensor approach is evident in

relating $\langle u_r \rangle^2$ to the principal axes of the electric field gradient (efg), which are in general rotated from the crystal axes. In the new reference frame (efg), $\langle U_r^2 \rangle$ becomes $\langle u_s^2 \rangle$. Then

(62) $\langle U_s^2 \rangle = \sum_r D^{(2)}(\{\alpha, \beta, \gamma\})_{sr} \langle U_r^2 \rangle$

where $D^{(2)}(\{\alpha, \beta, \gamma\})$ is the matrix of the irreducible representation of the rotation group, α, β, and γ being the "Euler angles" relating the coordinate axes in the two systems. This analysis is in principal possible for complex structures, but in practice unfortunately very difficult. The above description is a simplified version.

In general, one has a representation describing quantitatively the anisotropic f_a. This anisotropy is difficult to determine experimentally since its effect on the overall intensity pattern is usually small. It is observed on powders with completely random orientation(which cancels out other intensity factors and leaves only this term to account for differing intensity between two lines of a quadrupole doublet). Various models of vibrations in solids can relate f_a (averaged) to the Debye temperature. Unfortunately this Debye temperature cannot be assumed to be the same as the Debye temperature calculated from specific heat measurements, as the frequency of the vibrations affecting the f_a most strongly is not the "average" frequency used in specific heat interpretation.

The second effect of crystal orientation is the "crystal effect", which describes the transition probabilities as a function of the angle the incoming gamma ray makes with the principal axes of the field applied to the nucleus. This discussion, following the work of Wertheim (1964),

is limited to Fe^{57}, as this is the nucleus of primary mineralogic interest.

The electric field gradient at the nucleus is

(63) $$\frac{\partial^2 V}{\partial x^2} + \frac{\partial^2 V}{\partial y^2} + \frac{\partial^2 V}{\partial z^2} \equiv \nabla^2 V = 0$$

This can be described in terms of Vzz ($= \frac{\partial^2 V}{\partial z^2}$) (which we will define as the maximum efg) and the "asymmetry parameter" $\eta = \frac{V_{xx} - V_{yy}}{V_{zz}}$ where Vxx is chosen to be greater the Vyy so that η varies from zero to one. If $\eta = 0$, Vzz is an axis of rotation (3-fold or greater), and vice versa. If the nuclear quadrupole moment is known (+.28 barns for Fe^{57}), then its interaction with the efg is given by the Hamiltonian

(69) $$H = Q \cdot \nabla E = Q \cdot (-V_{ij})$$

The eigenvalues are

(65) $$E_Q = \frac{eqQ}{4I(2I-1)} \left[3m_I^2 - I(I+1)\right] (1+\eta^2/3)^{\frac{1}{2}}$$

$$m_I = I, I-1, \ldots -I$$

For Fe^{57}, I equals 3/2 and therefore m_I equals 3/2 or 1/2. The final value observed is E_Q, or the quadrupole splitting. It depends on the efg, which is related to nonspherical, relatively distant, charges by:

(66) $$q = q' (1 - \gamma_\infty)$$

where q' is the distant charge and $1 - \gamma_\infty$ is the antishielding factor, which may be computed from knowledge of the wave functions. The final result is

(67) $$\Delta E_Q = \tfrac{1}{2} e^2 q' Q (1-\gamma)(1 + \tfrac{\eta^2}{3})^{\frac{1}{2}}$$

This energy is not affected by any angular factors, so one would not expect the magnitude of the quadrupole splitting to be affected by

crystal orientation, and this is found to be the case.

The important factor with angular dependence turns out to be the transition probability. While it is the electric quadrupole moment which splits the energy of the excited I = 3/2 state in Fe^{57}, the observed transition is a magnetic dipole (M1) transition. (The Fe^{57} nucleus has a magnetic dipole moment). Other transitions are possible, including electric quadrupole, but turn out to be much less probable that the M1 transition. The dipole transitions have a well known angular dependence,

(68) $\frac{5}{3} - \cos^2\theta$ for $\Delta m = 0$

(69) $1 + \cos^2\theta$ for $\Delta m = \pm 1$

These factors apply to an incoming gamma ray at angle θ from the principal axis, here the z axis of the efg. The M1 transition from $\pm$ 3/2 has full circular polarization, while the one from $\pm$ 1/2 has 2/3 linear and 1/2 circular polarization. These give rise to the differences between the two peaks of a doublet. The intensity angular factors integrated over a sphere give equal intensity for the two lines, so a powdered randomly oriented crystallite will show a symmetric doublet, with equal intensities. However, one has to multiply the angular factor by the Mossbauer fraction f_a, obtaining

(70) $(1 + \cos^2\theta)\, f_a(\theta)$ for $\Delta m = \pm 1$

(71) $(5/3 - \cos^2\theta)\, f_a(\theta)$ for $\Delta m = 0$.

If f_a is anisotropic, then these factors integrated over a sphere <u>are not</u> equal. Thus a powdered sample can show whether there is anisotropy

in f_a and indicate its size, although it does not tell the orientation of the anisotropy relative to the crystal axes.

Further complications are added if there is a magnetic field, either internally or externally applied. This lifts the rest of the energy degeneracy and six peaks result. Fortunately, this is still a dipole transition and similar angular factors hold:

(72) $(3/2 \rightarrow 1/2) = (-3/2 \rightarrow 1/2) = 3(1 + \cos^2\theta)/2 \quad \Delta m = 1$

(73) $(1/2 \rightarrow -1/2) = (-1/2 \rightarrow 1/2) = (1 + \cos^2\theta)/2 \quad \Delta m = 1$

(74) $(1/2 \rightarrow 1/2) = (-1/2 \rightarrow -1/2) = 2\sin^2\theta \quad \Delta m = 0$

Here θ is the angle between the gamma wave vector and the magnetic field. If the magnetic field is parallel to the gamma wave vector, then one of the pairs of peaks disappears. This effect can be useful in simplifying spectra of magnetic materials.

With these considerations, it became important to determine if the presence of a prominent cleavage in orthopyroxene might be one of the factors causing asymmetry in intensity between high and low energy peaks of both M1 and M2 doublets. A simple experiment was designed to qualitatively investigate the possible effects. A sample of HCo was powdered and thinly spread on a flat surface, in order that as many fragments as possible would lie on the prominent (210) cleavage surface. This was picked up with tape in order to maintain the orientation. The tape was attached to a sample holder and run at room temperature in order to discover the asymmetry (if any) produced in the spectrum.

The resultant spectrum showed a large low energy peak and smaller

higher energy peak. The area, which should be 50% for M1 + M2 low energy peaks if symmetric, was instead 54.99%. The indication is that the Vzz direction, or highest electric field gradient, lies more within the plane of cleavage than perpendicular to it. This is not too surprising when one considers that the cleavage is an expression of weakly bonded planes, where electron density is likely to be lower. No attempt was made to investigate the M1 and M2 peaks separately, although they probably have somewhat different orientations of Vzz, and thus different responses to preferred orientation. The measured effect is likely that of M2 sites, which contain most of the iron in this sample.

Some preliminary work done with single crystal sections cut parallel and perpendicular to the cleavage, but from a different sample of orthopyroxene, tend to bear out the conclusions reached in the above experiment. A large and potentially fruitful area of study lies here uninvestigated.

BIBLIOGRAPHY

Bancroft, G.M., R.G.Burns, and R.H.Howie (1967) Determination of the Cation Distribution in the Orthopyroxene Series by the Mossbauer Effect. Nature v. 213, p. 1221-1223.

Boland, J., A. Duba, and A. Eggleton (1974) Kinetic and microstructural studies of magnesium-rich orthopyroxenes. J. Geol., v. 82, p.507-514.

Boyd, F.R. (1974) The Mantle Sample from the Kimberlites and an Estimated Geotherm. Trans. AGU, v.55, p.215.

Brown, William L (1971) Entropie de configuration, solution solide et structure cristalline. Bull. Soc. Fr. Mineral Cristallogr., 94, p. 38-44.

Buening, D.K., and P.R. Buseck (1973) The pO_2 dependence of vacancy formation in olivine (abstract). EOS Trans. AGU, v.54, p.498.

Burnham, C.W., Y. Ohashi, S. S. Hafner, and D. Virgo (1971) Cation distribution and Atomic Thermal Vibrations in an Iron-Rich Orthopyroxene Am. Min. v.56 p. 850.

Buseck, P.R., and S. Iijima (1974) Aspects of High Resolution Electron Microscopy of Minerals (Abstract). American Crystallographic Association, Annual Meeting, Program and Abstracts. ser. 2, vol. 2, p. 81.

Coughlin, J.P. (1954) Contributions to the Data on Theoretical Metallurgy. XII Heats and Free Energy of Formation of Inorganic Oxides. U.S. Bureau of Mines Bulletin, No. 542.

Darken, L.S., and R.W.Gurry (1945) The system iron-oxygen. I. The wustite field and related equilibria. J. Amer.Chem. Soc., v. 67, p. 1398-1412.

Deines, P., R. H. Nafziger, G. C. Ulmer, and E. Woermann (1974) Temperature-Oxygen Fugacity Tables for Selected Gas Mixtures in the System C-H-O at one Atmosphere Total Pressure. Earth and Mineral Sciences Experiment Station, The Pennsylvania State University, Bull. 88.

Denbigh, K. (1966) The Principles of Chemical Equilibrium. Cambridge University Press, Cambridge, G.B.

Dienes, G.J. (1955) Kinetics of Order-Disorder Transformations. Acta Met. v. 3, p.549-557.

Dowty, E., and D. Lindsley (1973) Mossbauer Spectra of synthetic hedenbergite-ferrosilite pyroxenes. Am. Min., v.58, p.850-868.

Duba, A., N. J. Boland, and A. E. Ringwood (1973) The electrical conductivity of pyroxene. J. Geol. v.81, p.727-735.

Dundon, R.W., and S.S.Hafner (1971) Cation disorder in shocked orthopyroxene. Science, v.174, p. 581-583.

Elliott, J.F., and M.Gleiser (1960) Thermochemistry for Steelmaking. Addison Wesley Publishing Co., Inc., Reading, Ma.

Evans, B.J., S.Ghose, and S.S.Hafner (1967) Hyperfine splitting of ^{57}Fe and Mg-Fe order-disorder in orthopyroxenes ($MgSiO_3$-$FeSiO_3$ solid solution). J. Geol., v.75, p.306-322.

Feynmann, R., R. Leighton, and M.Sands (1963) The Feynman Lectures on Physics. 3 vols. Addison-Wesley Publishing Co., Reading Ma.

Flynn, C.P. (1972) Point Defects and Diffusion. Clarendon Press, Oxford University Press, London.

French, B.M. (1966) Some geological implications of equilibrium between graphite and a C-H-O gas phase at high temperatures and pressures. Rev. Geophys., 4, p.223-253.

Ghose, S. (1962) The Nature of Mg^{2+} - Fe^{2+} order in some ferromagnesian minerals. Am. Min., v.47, p.388-394.

Ghose, Subrata.(1965) Mg^{2+} - Fe^{2+} order in an orthopyroxene, $Mg_{0.93}Fe_{4.07}Si_2O_6$. Z. Kristallogr., 122, p.81-99.

Ghose, S., and S.S.Hafner (1967) Fe^{2+} - Mg^{2+} Distribution in Metamorphic and volcanic orthopyroxenes. Z. Kristallogr. 125,p.157-162.

Gray, N.O. (1973) Kinetics of Fe-Mg Ordering in Orthopyroxenes. (Abstract) Trans. AGU, V.55, p. 467.

Grover, J. (1974) On calculating activity coefficients and other excess functions from the intracrystalline exchange properties of a double-site phase. Geochim. Cosmochim. Acta. v.38, p.1527-1548.

Grover, J.E., and P.M. Orville (1969) The partitioning of cations between coexisting single and multisite phases with application to the assemblages: orthopyroxene-clinopyroxene and orthopyroxene-olivine. Geochim. Cosmochim. Acta, v.33, p.205-226.

Harris, J.W., and E.R.Vance (1974) Studies of the Reaction between Diamond and Heated Kimberlite. Contr. Mineral Petrol., v.47, p.237-244.

Holm, J.L., and O.J.Kleppa (1968) Thermodynamics of disordering in albite. Am. Min, 53, p.123-133.

Imbert,P., and E, Martel (1965) Etude par l'effet Mossbauer de la Structure magnetique du chromite de fer $FeCr_2O_4$ a basse temperature. Compte Rendus Acad. Sc. Paris, v.261, p.5404-5407.

Khristoforov, K.K., L.P.Nikitina, L.M.Krizhamskii, and S.PEkimov (1974) Kinetics of iron (2+) ion disordering in structure of rhombic pyroxenes. Doklady, Earth Science Sections, v.214,March 1975,p. 165-167.

Kroger, F.A. (1964) The Chemistry of Imperfect Crystals. John Wiley and Sons, N.Y. 1039 p.

Lacey, E. D. (1965a) "Factors in the Study of Metamorphic Reaction Rates", in, Controls of Metamorphism, ed. W. S. Pitcher and G. W. Flinn. John Wiley and Sons, New York.

Lacy, E.D. (1965b) Configuration change in silicates with particular reference to network structure. Acta Crystallogr. 18, p141-150.

McGetchin, T. R., and G. W. Ullrich (1973) Deep-Seated Xenoliths: Observed Terrestrial Abundance, Distribution and Emplacement in Some Maars and Diatremes with Inferences for the Moon, Mars, and Venus. JGR v.78, p.1833-1853.

Marzolf, J.G., J.T.Dehn, and J.F.Salmon (1967) Mossbauer studies of tektites, pyroxnes, and olivines. Adv. Chem. Ser. v. 68, p.61-85.

Matsui, Y., and S. Banno (1965) Intracrystalline exchange equilibrium in silicate solid solutions. Proc. Jap. Acad. v.41, p.461-466.

Muan, H., and E.F.Osborn (1965) Phase Equilibria Among Oxides in Steelmaking. Addison-Wesley Publishing Co., Reading, Ma.

Mueller, R.F. (1962) Energetics of certain silicate solid solutions. Geochim. Cosmochim. Acta, v.26,p.581-598

Mueller, R.F. (1967) Model for order-disorder kinetics in certain quasi-binary crystals of continuously variable composition. J. Phys. Chem.Solids 28, p.2239-2243.

Mueller, R.F. (1969) Kinetics and Thermodynamics of Intracrystalline Distributions, Min. Soc. Am. Spec. Pap. 2, p.83-93

Mueller, R.F. (1970) Two-step mechanism for order-disorder kinetics in silicates. Am. Min., v.55, p.1210-1218.

Nafziger, R., G. Ulmer, and E. Woermann (1971) Gaseous Buffering for the Control of Oxygen Fugacity at One Atmosphere. Research Techniques for High Pressure and High Temperature, Gene C Ulmer, ed. Springer-Verlag, New York.

Navrotsky, A. (1971) The Intracrystalline Cation Distribution and the Thermodynamics of Solid Solution Formation in the System $FeSiO_3$ - $MgSiO_3$. Am. Min., v.56, p.210-211.

Nitsan, U. (1974) Stability Field of Olivine With Respect to Oxidation and Reduction. JGR, v.79, p.706-711.

Prigogine, I. (1967) Introduction to Thermodynamics of Irreversible Processes. Interscience Publishers, New York. 147 p.

Robie, R.A., and D.R.Waldbaum (1968) Thermodynamic properties of minerals and related substances at 298.15°K (25.0°C) and one atmosphere (1.013 bars) pressure and at higher temperatures. U.S. Geol. Survey Bull., 1259

Ross, S.L. (1964) Differential Equations. Blaisdell Publishing Co., Waltham, Ma.

Saxena, S.K. (1973) Thermodynamics of Rock-Forming Crystalline Solutions. Springer-Verlag, New York. 188 p.

Saxena, S.K., and S.Ghose (1971) Mg^{2+} - Fe^{2+} order-disorder and the thermodynamics of the orthopyroxene-crystalline solution. Am. Min., v.56, p.532-559.

Sato, M. (1971) Electrochemical Measurements and Control of Oxygen Fugacity and Other Gaseous Fugacities with Solid Electrolyte Sensors. in, Ulmer, G.C., Research Techniques for High Pressure and High Temperature. Springer Verlag, New York.

Shewmon, Paul G. (1963) Diffusion in Solids, McGraw Hill Book Co., New York. 203 p.

Smith, J.V. (1969) Crystal structure and stability of the $MgSiO_3$ polymorphs; physical properties and phase relations of Mg, Fe pyroxenes. Min. Soc. Am. Spec. Pap. 2, p.3-29.

Smith, J.V., and Ribbe, P.H. (1969) Atomic Movements in plagioclase feldspars: a kinetic interpretation. Contr. Min.Pet. v.21, p. 157-202.

Smyth, J.R. (1969) Orthopyroxene-high-low clinopyroxene inversions. Earth Planet. Sci. Lett. 6, p.406-407.

Smyth, J.R. (1970) High temperature single crystal x-ray studies of natural orthopyroxenes (Abstract). Am. Min., 55, p. 312.

Smyth, J.R. (1971) Protoenstatite: a crystal structure refinement at 1100°C. Z. Kristallogr. 134, p. 262-274.

Smyth, J.R. (1973) An orthopyroxene structure up to 850°C. Am. Min., 58, p. 636-648.

Smyth, J.R., and C.W.Burnham (1972) The crystal structures of high and low clinohypersthene. Earth Planet. Sci. Lett. 14, p.183-189.

Stockler, H.H., and H.Sano (1970) Mossbauer Effect Studies of Lattice-Dynamic Anisotropy and Line Asymmetry in Semiconductor and Organometallic Tin Compounds; in, Mossbauer Effect Methodology, v.5, ed. I Gruverman. Plenum Press, New York and London.

Turner, F.J., H.Heard, and D.T.Griggs (1960) Experimental deformation of enstatite and accompanying inversion to clinoenstatite. XXI Int. Geol. Cong. Copenhagen, v.18, p.399-408.

Vineyard, G.H. (1956) Theory of Order-Disorder Kinetics. Phys. Rev., v. 102, p.981-992.

Virgo, D., and S.S.Hafner (1969) Fe^{2+} - Mg disorder in heated orthopyroxenes. Min. Soc. Am. Spec. Pap. 2, p.67-81.

Virgo, D., and S.S. Hafner (1970) Fe^{2+}, Mg order-disorder in natural orthopyroxenes. Am. Min., 55, p.201-223.

Warren, B.E., and D.I.Modell (1930) The structure of enstatite, $MgSiO_3$. Z. Kristallogr. 75, p.1-14.

Wallis, W.A., and H.V.Roberts (1956) Statistics, A New Approach. The Free Press, New York, 646 p.

Wertheim, G.K. (1964) Mossbauer Effect: Principles and Applications. Academic Press. New York and London. 116 p.

Whipple, E.R. (1973) Quantitative Mossbauer Spectra and Chemistry of Iron. Unpubl. PhD thesis, M.I.T., Cambridge, Ma.

Williams, A.F. (1932) The Genesis of the Diamond. v. 1. Ernest Benn Ltd. London. 352 p.